DEPARTMENT OF CHEMICAL SCIENCES
COLLEGE OF SCIENCES
OLD DOMINION UNIVERSITY
NORFOLK, VIRGINIA 23529

LOW PRESSURE GAS FLOW ANALYSIS THROUGH AN EFFUSIVE INLET USING MASS SPECTROMETRY

David R. Brown

and

Kenneth G. Brown, Principal Investigator

Final Report
For the period ended December 31, 1987

Prepared for the
National Aeronautics and Space Administration
Langley Research Center
Hampton, Virginia 23665

Under
NASA Contract NAS1-17993
Task Authorization No. 74
Dr. G.M. Wood, Jr., Technical Monitor
IRD-GEN Res Instrn Br

May 1988

DEPARTMENT OF CHEMICAL SCIENCES
COLLEGE OF SCIENCES
OLD DOMINION UNIVERSITY
NORFOLK, VIRGINIA 23529

LOW PRESSURE GAS FLOW ANALYSIS THROUGH AN EFFUSIVE INLET USING MASS SPECTROMETRY

David R. Brown

and

Kenneth G. Brown, Principal Investigator

Final Report
For the period ended December 31, 1987

Prepared for the
National Aeronautics and Space Administration
Langley Research Center
Hampton, Virginia 23665

Under
NASA Contract NAS1-17993
Task Authorization No. 74
Dr. G.M. Wood, Jr., Technical Monitor
IRD-GEN Res Instrn Br

Submitted by the
Old Dominion University Research Foundation
P.O. Box 6369
Norfolk, Virginia 23508

May 1988

ABSTRACT

LOW PRESSURE GAS FLOW ANALYSIS THROUGH AN EFFUSIVE INLET USING MASS SPECTROMETRY

David Robert Brown
Old Dominion University, 1988
Director: Dr. Kenneth G. Brown

A mass spectrometric method for analyzing flow past and through an effusive inlet designed for use on the tethered satellite and other entering vehicles is discussed. Source stream concentrations of species in a gaseous mixture are determined using a calibration of measured mass spectral intensities versus source stream pressure for standard gas mixtures and pure gases. Concentrations are shown to be accurate within experimental error. Theoretical explanations for observed mass discrimination effects as they relate to the various flow situations in the effusive inlet and the experimental apparatus are discussed.

TABLE OF CONTENTS

LIST OF TABLES

LIST OF FIGURES

LIST OF FIGURES (cont.)

LIST OF FIGURES (cont.)

FIGURE Page

LIST OF MATHEMATICAL SYMBOLS

λ - mean free path
r - capillary radius
l - capillary length
L - capillary length/radius
P_1 - source stream or upstream pressure
P_2 - downstream pressure
P_{MS} - mass spectrometer pressure
P_T - total pressure
I_i - mass spectrometric intensity of species i
S_i - sensitivity of species i
G_D - flow due to gaseous self-diffusion
G_S - flow due to surface diffusion
G - total flow
W_D - dimensionless flow due to diffusion
W_P - dimensionless flow due to drift
W - specific or dimensionless flow
MCP - microchannel plate
v - mean speed of a molecular or atomic species
n - number of molecular or atomic species
m_i - mass of species i
f_D - separation factor for diffusive flow
Z_D - separation efficiency due to diffusion
Z_S - separation efficiency due to surface diffusion
F_i - product of vibrational force constants of i
ϵ_i - energy of adsorption of species i
E_i - activation energy for a random walk
X_i - mole fraction of species i
k_i - calibration constant for species i
K - ratio of calibration constants
[i] - concentration of species i
E' - enrichment ratio
a,b,c - fitting constants
Γ_i - product of adsorptive partition functions

INTRODUCTION

Project History

The purpose of this thesis is to present a mass spectrometric method for determining the gaseous composition of a vehicle boundary layer. The particular vehicles for which this model method is being developed are the tethered satellite and other re-entry vehicles which fly about 90 km above the earth's surface and higher.

The boundary layer is the gaseous region around a vehicle with flow rates less than that of the bulk region (see Figure 1). Knowing the properties of the boundary layer is essential for vehicle design and theoretical modeling of the associated flight parameters such as re-entry angles and heat loads. To date, these models use physical properties alone (i.e. temperature and pressure measurements at the vehicle's surface) and, as such, neglect how the gaseous composition of the boundary layer affects the modeling. It has been suggested that existing theoretical models could be improved by including viscous and real-gas effects, effects requiring that the boundary layer composition be determined (1).

Due to restrictions imposed by the vehicle and its

Figure 1. Drawing of a boundary layer associated with an aircraft in flight.

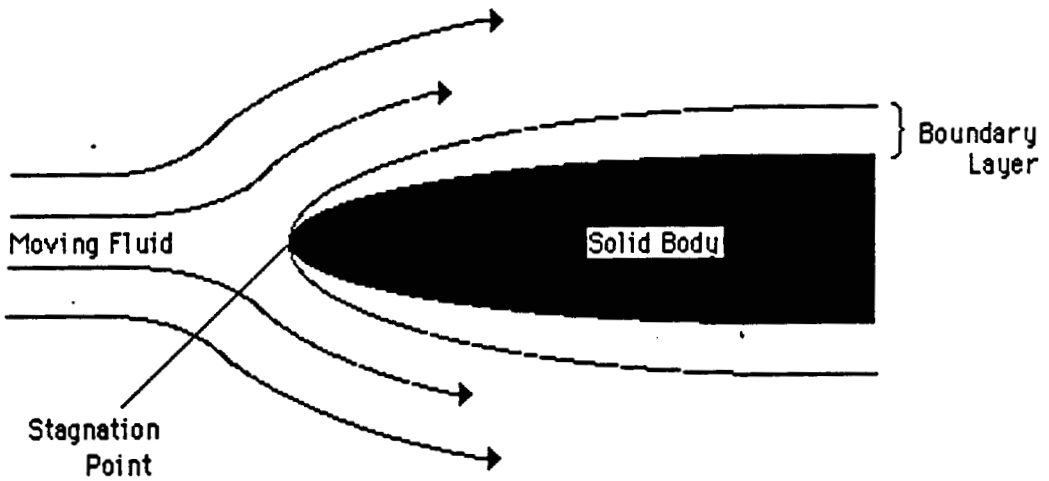
Boundary
Layer
Moving Fluid
Solid Body
Stagnation
Point

environment, the upper atmosphere, the inlet for the mass spectrometer (MS) must meet requirements which do not exist for traditional MS sample inlets. It will beinstructive to discuss these requirements and how they relate to (1) the choice of sample inlet and (2) the accurate determination of the boundary layer composition.

The first requirement of the MS inlet is that it sample the boundary layer in a nonintrusive manner. The tethered satellite is a research vehicle carrying several instruments for analysis of the upper atmosphere. Nonintrusive sampling insures that (1) the sample is representative of the boundary layer alone and not the surrounding bulk region, (2) the measurements made downfield of the MS inlet are not affected, and (3) the flight performance of the tethered satellite or other vehicle is not affected. A nonintrusive inlet does not perturb the flow field around the vehicle. Perturbation will result from either flow sinks or large pressure drops in the flow field. Flow sinks can be prevented by mounting the MS inlet flush with the surface, and pressure drops can be prevented by sampling in an effusive (non-pumping) manner. The envisioned on-board MS system has been discussed previously and as presently envisioned, the sample inlet will be mounted flush with the surface of the tethered satellite in a location normal to the flow of the boundary layer (2).

Effusive flow of a gaseous species through an inlet results from the species' random collisions with the inlet resulting in passage through the inlet's orifice. Molecular speeds, therefore, dictate the rates of effusive flow for a given species. Effusive flow occurs only under certain conditions defined by the dimensions of the orifice relative to the flow regime of the gas (molecular, slip, or transition). The flow regime is determined by the pressure of the gas. The pressure range examined experimentally is 2 torr or less and should encompass the range of pressures likely to be encountered in the upper atmosphere. Over this range, effusive flow can occur only through small diameter openings approximately 0.010 mm or less. Where a pinhole or capillary inlet of this size could provide effusive flow over the given pressure range, it is unlikely that at the lower pressures enough sample would be admitted into the MS to be detected. Increasing the number of small diameter openings, however, would allow more sample to enter the MS while retaining the characteristic effusive flow of a single capillary. This was confirmed experimentally by Knudsen (3).

For the purpose of this study a Galileo Electro-optics Corp. microchannel plate (MCP) was used as the sample inlet. An MCP is an array of short, small diameter capillaries in a thin glass plate, commonly

found in signal amplification devices (see Figure 2). The manufacturing of an MCP involves heating and stretching bundles of glass tubes until their openings are of capillary dimension. The bundles fuse into a single mass during this process. Slicing the mass perpendicular to the axes of the capillaries gives thin plates which are the MCP's. The MCP used in this study had 10 micron-diameter capillaries or 10 micron centers, with a number density of about $10^5/cm^2$ of surface area. Preliminary results indicate that this number of capillaries does not create a high enough pressure drop across the high- and low-pressure sides of the inlet to maintain the required operational pressure of $< 10^{-5}$ torr in the MS ion source. In order to increase the pressure drop created by the MCP, the majority of the capillary openings were masked with a stainless steel pinhole sealed to the MCP surface with a thin layer of teflon. The resulting MCP-mask combination leaves only a small array of capillary openings exposed to the sample gas, the actual number being dictated by the diameter of the pinhole.

Another restriction on sampling the boundary layer results from the gas property profile of the boundary layer. Because the gas properties vary dramatically within the boundary layer at small distances from the surface of the vehicle, it is necessary to sample at the

Figure 2. Drawing of a microchannel plate, MCP, showing the capillary density and capillary dimensions.

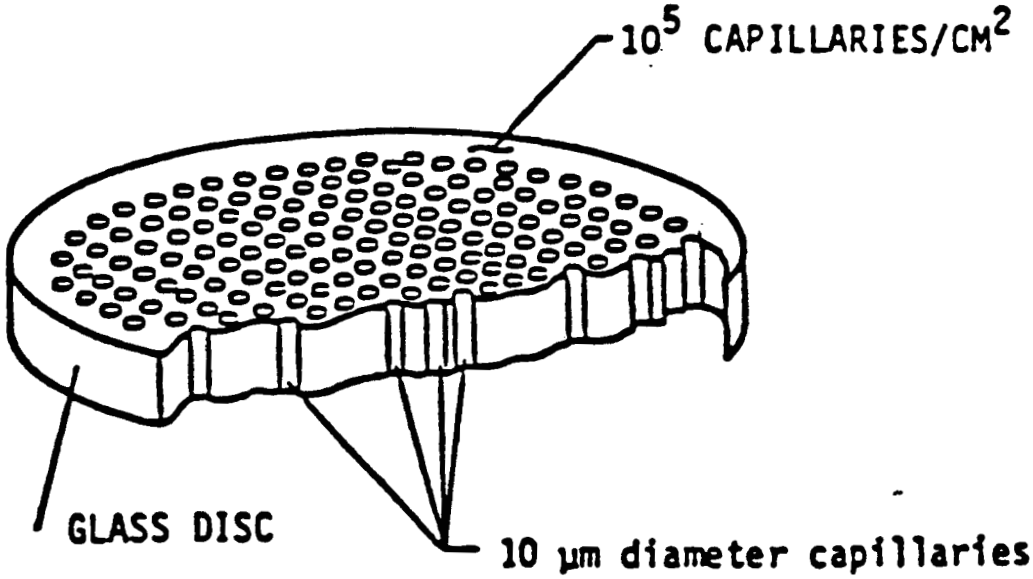

THE EFFUSIVE INLET

surface of the vehicle (1). In the past, sampling techniques employed inlets which were either intrusive or sampled in a location not characteristic of the composition at the surface the vehicle. Such inlets included pitot probes, flush orifices, stripper probes (4), and aerodynamic jet probes (5). Calculations performed by Brown considering the location and the free area of the MCP, on the other hand, predict that sampling with an MCP will occur maximally to 10^{-6} cm into a 2-cm boundary layer for the given flight regimes (6). Therefore, theory suggests sampling will remain at the surface of the vehicle with negligible mixing, as desired.

In summary, the MCP-mask combination proves an outstanding candidate for an inlet to the on-board MS system based on its potential ability to provide effusive, nonintrusive sampling of gaseous species at the surface of a vehicle within the boundary layer.

Statement of Problem

It is commonly known that gas may be quantitatively altered in composition by flowing through a capillary effusively. Mass discrimination effects arising from flow differences between gaseous species as they relate to the MCP must be accounted for if accurate compositions are to be obtained. As predicted by kinetic theory, the degree to which mass discrimination occurs upon flowing

through a capillary is a function of (1) the relative masses of the species in the gas; (2) the relative force of attraction between the species and the material of which the capillary is made; (3) the dimensions of the capillaries; and (4) the flow regime of the gas passing through the capillary. Calibration of the MCP and the associated apparatus with some degree of understanding of how the flow effects might alter the composition of a sampled gas is necessary to account for alterations in sample gas composition. With alterations taken into account, the concentration of the species as they are in the boundary layer can be determined. We are interested in knowing if such a calibration is possible and whether or not the discrimination effects of the MCP are similar to that observed with a pinhole.

THEORY

To better understand what behavior a gaseous mixture might be expected to demonstrate upon passing through the proposed sample inlet, it will be instructive to survey some theory of capillary flow. The boundaries of each flow regime as a function of mean free path to radius ratio, λ/r, are defined in the table below.

FLOW REGIME	λ/r
Viscous	$\lambda/r < 10^{-1}$
Slip or Transition	$10^{-1} < \lambda/r < 10$
Molecular	$10 < \lambda/r$

These definitions are approximate mainly because little is known about the slip flow regime making it difficult to assign definite limits between regimes. In the molecular flow regime pressures are low enough for $\lambda >> r$. Here collisions occur only between the individual molecules and the capillary wall; there are no molecule-molecule collisions. As the pressure increases, the flow regime changes from molecular to slip ($\lambda \approx r$). Here molecule-molecule and molecule-wall collisions are on the same order of magnitude. At the highest pressures ($\lambda << r$), molecule-molecule collisions far outnumber the

molecule-wall collisions.

Knudsen developed the first kinetic theory expressions for capillary flow in the molecular flow regime (3). He proposed that the driving force for flow is gaseous self-diffusion under and dependent on a pressure gradient established by the pressures at either end of the capillary. The expression for the mean flow due to diffusion, G_D, obtained by Knudsen in the ideal limit of molecular flow is

$$G_D = -(2vr/3)(dn/dx) \qquad (1)$$

where the capillary axis is coaxial with the x axis, v is the mean speed of a molecule, and n is the number of molecules. The first parenthenthetical term is the diffusion coefficient D. This equation was confirmed by data obtained for bundles of capillaries (3,7,8). Knudsen plotted G_D as a function of λ/r and observed a flow minimum occurring in the slip flow regime. His equation only approximately predicted the location of the minimum.

In attempting to theoretically explain the flow minimum observed by Knudsen and to derive an expression for G_D over all flow regimes, Pollard and Present (9) and later Scott and Dullien (10) proposed that D is a function of pressure and obtained flow equations based on

this function, D(P). Their equation correctly predicted a flow minimum, but failed to give the correct λ/r at which the flow minimum occurred. The reason for their incorrect prediction is that flow is a function of more that just diffusion.

Because molecules diffuse independently of one another in the molecular flow regime, making a ratio of flows from equation 1 for the species in a binary mixture shows that the maximum or ideal separation factor, f_D, for diffusive flow is

$$f_D = G_i/G_j = v_i/v_j = (m_j/m_i)^{1/2} \qquad (2)$$

where m_i and v_i are the mass and mean speed of species i. Using the equations developed by Pollard and Present, Pollard and DeBethune (11) later determined the separation efficiency, Z_D, of capillary flow as a function of pressure for a binary mixture from which f_D could be calculated. Pollard and DeBethune's treatment reduced to the same simple expression as that obtained by Knudsen for the ideal limit of molecular flow and showed additionally that f_D decreased as the pressure increased through the molecular and slip flow regimes, diminishing to zero before reaching the viscous flow regime. The decrease in f_D indicates that a binary mixture will show an enrichment in the lighter species with an upper bound

given by equation 2 in the limit of molecular flow. The reason for the lack of mass enrichment at higher pressure flows (in the viscous flow regime) is mixing resulting from the numerous collisions between unlike molecules. Note that results based on gaseous self-diffusion always show enrichment in the lighter species.

The first accurate expression for flow through a capillary of arbitrary length/radius, L, and over all flow regimes was obtained by Lund and Berman (12) using a semi-empirical approach. Their expression correctly explained the flow differences between species of a binary mixture by dividing the flow into diffusive and drift components, rather than by making D a function of pressure as others had done. The expression for the total flow G obtained by Lund and Berman is

$$G = [(1/4)\pi r^2 v(P_1 - P_2)]W \qquad (3)$$

where $P_1 - P_2$ is the pressure drop across the capillary and W is the total dimensionless flow, expressed by the relation

$$W = W_D + W_P \qquad (4)$$

where the subscripts D and P refer to the diffusive and the drift components of W, respectively. The quantity W

depends on L and the intermolecular forces between molecules and must be determined, in part, from experimental data. The results show that W_D decreases logarithmically as the pressure increases from zero, and that W_p is zero at zero pressure and increases as the pressure increases. As a result, W_D controls W at lower pressures, and W_p controls at higher pressures (see Figure 3).

It has already been shown that diffusive flow contributes to mass discrimination at lower pressures (i.e. the molecular and slip flow regimes). It can be shown from Lund and Berman's results that the drift component of flow, on the other hand, is negligible in contributing to mass discrimination at lower pressures. From their results, it is evident that drift flow controls at higher pressures (slip and viscous flow regimes) whereas diffusive flow controls at lower pressures (molecular and slip flow regimes). As mentioned previously, in the slip flow regime molecule-molecule collisions are on the same order as molecule-wall collisions. We must then consider a gaseous mixture to possess an average λ as the pressure increases through the slip flow regime. Therefore, as drift flow becomes controlling, differences between species in a mixture considered in W become negligible and therefore unable to contribute to mass discrimination. This follows the

Figure 3. Plot of W_D and W_P and the sum, W, obtained by Lund and Berman; the axes are defined in reference 12.

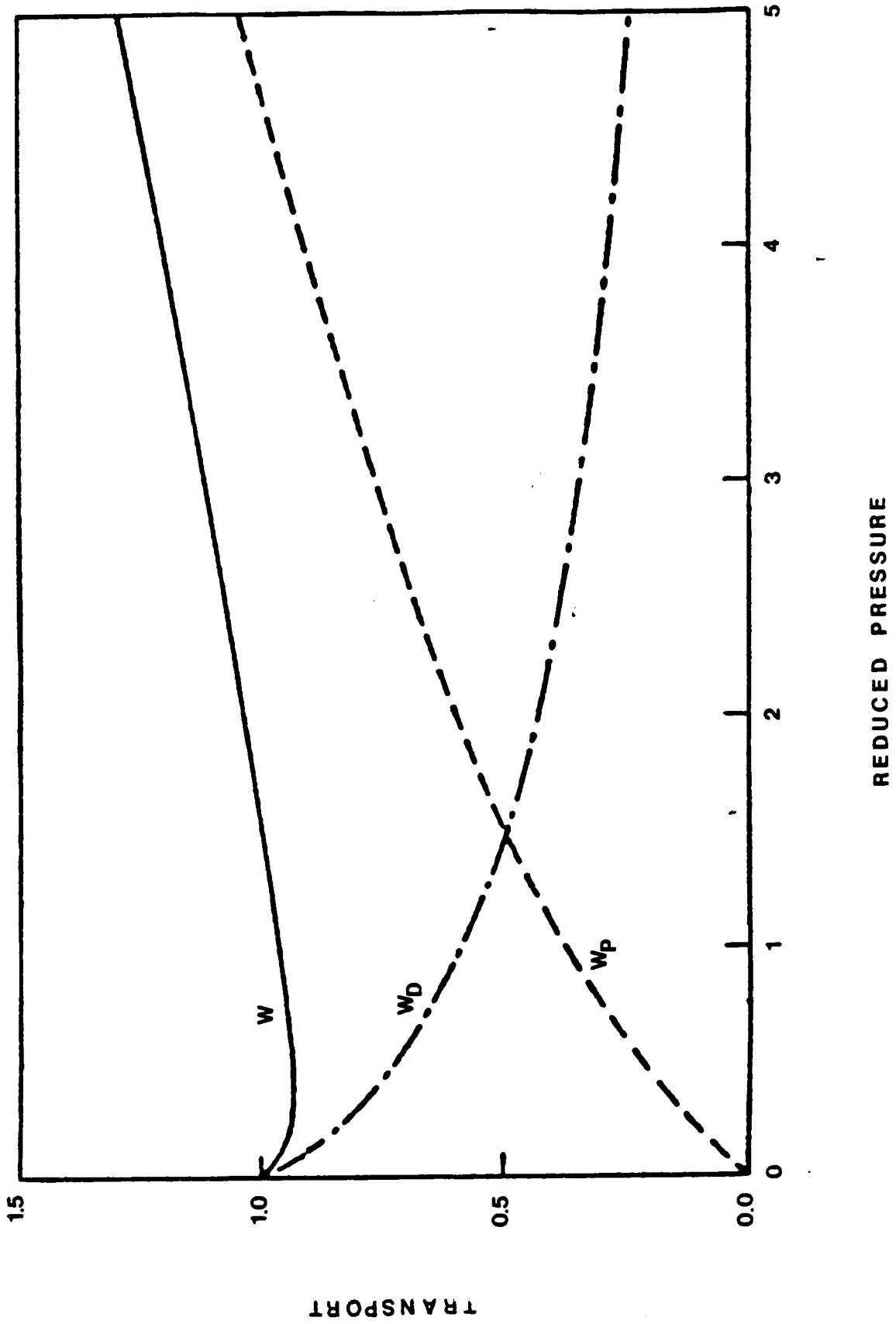
W
W_D
W_P
1.5
1.0
0.5
0.0
0
1
2
3
4
5
TRANSPORT
REDUCED PRESSURE

experimental observations for flow of binary mixtures through capillaries, where the degree of separation of species of different mass decreases to zero at the high λ/r-limit of the slip flow regime.

As mentioned earlier, surface diffusion of species capable of adsorbing to the inlet might contribute to mass enrichment. Ishida et. al. (13) divided G into diffusive and surface diffusive components, the former having been obtained by Pollard and DeBethune. They found that the separation efficiency due to surface diffusion, Z_S, was given approximately by

$$Z_S \approx (\Gamma_i/\Gamma_j)(m_j/m_i)^{1/2} \tag{5}$$

where Γ_i/Γ_j is a product of the partition functions associated with surface adsorption, given by

$$\Gamma_i/\Gamma_j = \exp[(\epsilon_i - E_i)/kT]/\exp[(\epsilon_j - E_j)/kT] \cdot \sqrt{(F_j/F_i)} \tag{6}$$

where ϵ is the energy of adsorption, E is the energy of activation necessary to make a random walk to the next adsorption sight, and F is the product of the vibrational force constants parallel and normal to the surface. For monatomic species, $\sqrt{(F_j/F_i)} = 1$ as monatomic species do not vibrate thus reducing equation 6 to the exponential factors. Equations 5 and 6 suggest that mass enrichment

will favor the species with the higher value for $\Gamma_i/\sqrt{m_i}$. Flow due to surface adsorption therefore makes it possible for the species in a binary mixture with the higher mass to be enriched, contrary to most theory.

Ishida compared separation efficiencies obtained by them with those obtained by Pollard and DeBethune for isotopes of uranium hexafluoride. The data showed that Ishida's equations for the separation efficiency were in better agreement with the experimentally obtained data than were Pollard and DeBethune's equations. Where Ishida's expression for Z_S is quite similar that for pure molecular flow obtained by Knudsen, it still shows that mass enrichment depends on surface diffusion.

From the above discussion we can conclude that the sample inlet may introduce mass discrimination effects as dictated by λ/r. G_D and G_S contribute to the total flow, G, but drift flow does not contribute. It should be noted that the afore-discussed theory assumes a steady-state system. A steady-state condition cannot be assumed on the tethered satellite, and it is unlikely that flow effects at the sample inlet surface created by flight can be neglected. To the best of the authors knowledge, however, there is no literature on the mass discrimination effects created by flow conditions before passage through an inlet.

EXPERIMENTAL

Apparatus

The experimental setups used to simulate the boundary layer relative to the sample inlet are shown in Figures 4 and 5. The source stream is created simply by flowing a sample gas through a 1/4-inch stainless steel tube perpendicular to the axis of the sample inlet. In Figure 4 the sample inlet is in direct contact with the flowing source stream or model boundary layer. In Figure 5 the sample inlet is recessed from the source stream by approximately 4 in. of 1/4-in. stainless steel tubing. The sample gas passes from the sample inlets to an Extrel Model C-50 quadrupole MS via 7 in. of 1/4-in. stainless steel tubing. At the MS the sample gas passes to the ion source via a 6-in. quartz tube.

The pressure of the gas is measured upstream (P_1) and downstream (P_2) of the inlet using separate Barocel absolute pressure gauges. Within the mass spectrometer, downstream of the ion source the MS pressure, P_{MS}, is measured using an ion gauge. The source stream flow (G) is measured upstream of the inlet using a mass flowmeter. The intensities (I_i) of the m/e at which the gaseous species are located are measured using the MS. The MS

Figure 4. Flow-by configuration of the Extrel Model C-50 MS showing the location of the sample inlet and the pressure measurements relative to the direction of flow.

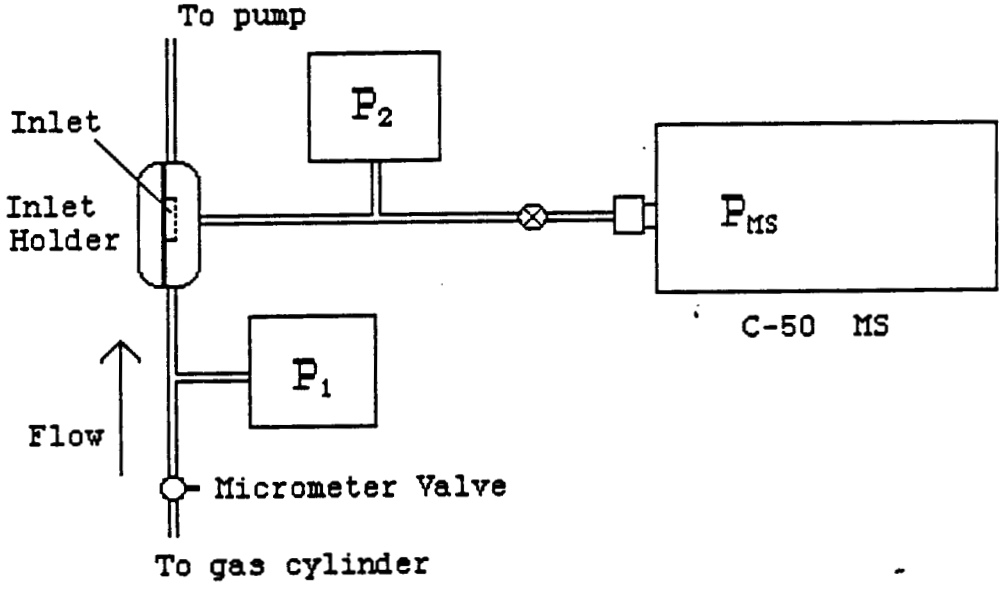
To pump
Inlet
Inlet Holder
P_2
P_{MS}
C-50 MS
P_1
Flow
Micrometer Valve
To gas cylinder

Figure 5. Straight-through configuration of the Extrel Model C-50 MS showing the location of the sample inlet and pressure measurements relative to the direction of flow.

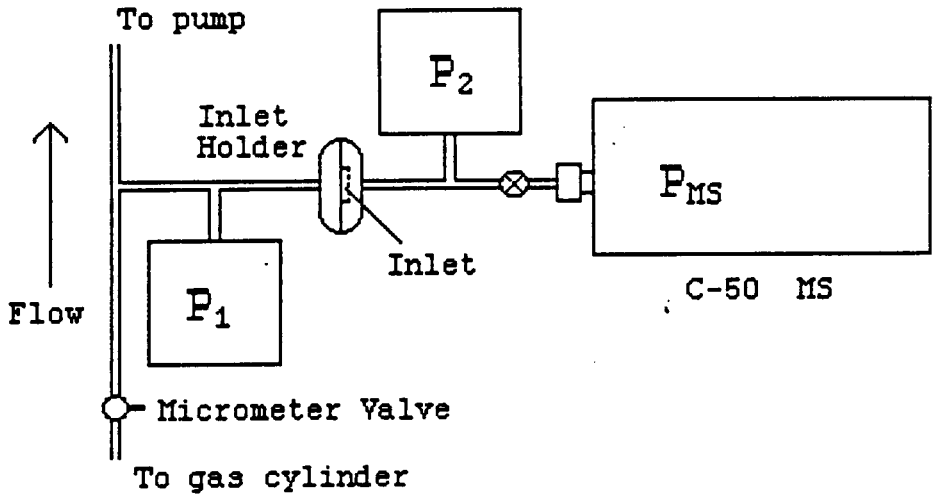
To pump
P_2
Inlet
Holder
P_{MS}
Inlet
C-50 MS
Flow
P_1
Micrometer Valve
To gas cylinder

and the pressure gauges are interfaced to an IBM Series 9000 microcomputer for data collection, storage, and computation. The application program will be discussed later.

Figure 6 shows an alternative configuration used in later and ongoing research which is similar to those found in Figures 4 and 5. The sample inlet is in direct contact with the perpendicularly flowing source stream as in Figure 4. The sample inlet itself, however, is in direct contact with the MS ion source, so a sampled gas passes from the sample inlet directly into the ion source with no interfering tubing. In this setup the MS is a UTI Precision Mass Analyzer used primarily for industrial applications and is completely computer controlled. In this configuration P_2 is P_{MS}, and this pressure is determined by the MS detector, an internal ion counter. Because the total number of ions at a given m/e is counted, I_i for each species i is a partial pressure.

The MCP's which we coded as MCP-025 and MCP-CB were donated by Galileo Electronics Corp. Two types of glass plate were characterized: (1) MCP-025, a one-inch diameter, polished, transparent plate, 0.40 mm thick with an average channel diameter of 0.010 mm and a channel density of approximately 7500 mm^{-2} and (2) MCP-CB, a one-inch diameter plate coated with a conducting material having an opaque, mirror-like surface, 0.40 mm thick with

Figure 6. UTI Precision Mass Analyzer showing the location of the sample inlet and pressure measurements relative to the direction of flow. Note that the sample gas passes directly into the MS ion source.

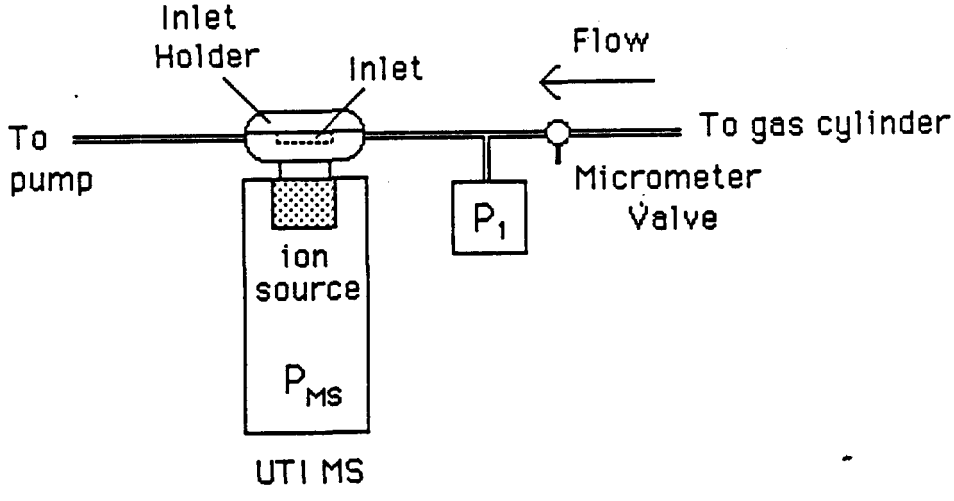
Inlet
Holder
Inlet
Flow
To
pump
To gas cylinder
Micrometer
Valve
P_1
ion
source
P_{MS}
UTI MS

channel openings averaging 0.0076 mm in diameter (probably approaching 0.009 mm in diameter at the center of the channel's length) and having a channel density of approximately 8000 mm^{-2}. The dimensions of the capillaries were determined using micrographs of the MCP's. The masks themselves were 0.025-0.050 mm thick with pinhole diameters ranging in size from 0.010-0.10 mm and were obtained from Optimation Corp.

Methodology

With the sample inlet in the holder, a typical experimental run proceeded by setting P_1 of the source stream gas (either a pure or a mixture gas) using an adjustable micrometer valve and measuring the resulting P_2, P_{ms}, G, and I_i. The measurements were recorded for a series of increasing P_1 for each gas. A series of pure and mixture gases were tested on several MCP-mask combinations to compare potential mass discrimination effects. Early in the research, this series included pure Ne, pure Kr, and a mixture of 9.71% Ne and 9.77% Kr in N_2 obtained from Scott Specialty Gases. For the sake of calculating concentrations, later experimental test gases included the following gases obtained from Air Products Specialty Gases: (1) 9.93% Ne in N_2 (2) 9.85% Kr in N_2 (3) 52.5% Ne in Kr and (4) 5.08% Ne and 14.9% Kr in N_2. Ne and Kr were chosen over other gases because of their large mass difference to enhance observed mass

discrimination effects. These gases were tested for the experimental setups shown in Figures 4 and 5. For the setup in Figure 6, the gases tested (also obtained from Scott) were (1) 3.033% CO_2 in air, (2) 7.55% CO_2 in air, and (3) 15.44% CO_2 in air. The composition of all gases was verified using GC. The Ne-Kr-N_2 series mentioned above is presently being tested on the UTI setup, but the data will not be included here.

C-50 COMPUTER PROGRAM

As mentioned earlier, the C-50 MS and the pressure gauges were interfaced to an IBM System 9000 for collection, computation, and storage of data. The program can be found in Appendix A. This section explains the structure of the controlling computer program. Before beginning it should be kept in mind that where the program was made as general and amenable to modification as possible to MS applications, it was written for the specific purposes of this research. In general, the program is divided into subroutines directed by a main program or menu. The subroutines in the menu are called "commands" and will be referred to as such throughout the rest of this section. The listing of the menu (290-400)[1], shown in Figure 7, allows scan parameter setup, data observation, data plotting, pertinent calculations, data storage, and ion gauge zeroing.

Menu

The program begins by requesting that the user enter the file in which the data will be stored. If this file already has data in it, then the computer reads the old

---

[1] In the rest of this section the numbers in parenthesis refer to the actual line numbers of the program to be found in Appendix A.

Figure 7. Actual CRT listing of the main menu in the computer program which takes data from the Extrel Model C-50 MS.

(1) Scan spectrum with new parameters
(2) Scan spectrum with same parameters
(3) Change mass range
(4) Display data
(5) List table of current results
(6) Choose major peaks again
(7) Plot results at CRT
(8) File results
(9) Sensitivity calculations and hard copies
(10) Hard copy of results
(11) Set zero-point for ion gauge
(12) Exit

Choose a command by pressing the number

data into the arrays defined for the data and counts the total number of data points. This feature allows old data files to be called up for reviewing. After opening and/or reading a file into the appropriate arrays (150-250), the program displays the menu. Commands 1-3 allow setup of all or some of the scan parameters. Commands 4-7 allow observation of the data in various ways: all intensities over the mass-to-charge (m/e or amu) range of the spectrum, detectable peak intensities of a given amu, or plots of intensities (or sensitivities) versus various pressure measurements. Commands 8-10 allow calculation, printing, and storage of data. Command 11 allows zeroing of the ion gauge when necessary. And command 12 exits the program.

The menu works as follows. A command in the menu is actuated by entering the number preceding the command. The program does this using an ON GOTO statement. This statement passes control from the menu to the location in the program where the command is carried out. Upon completion of the command, control is returned to the menu via a GOTO statement at the end of each subroutine. The program is then capable of executing other selections. It should be noted that before returning to the menu the operator has the option of exiting the program (270).

Scan Parameter Setup

Command 1 allows setup of all scan parameters including documentation and executes the scan. The documentation requested includes the date, the gas or gas mixture being used, the m/e of the species in the gas, and any conditions that may vary for a given setup (450-510). More permanent documentation including the MCP-mask combination used, the configuration used, and the MS parameters are stored in the program permanently and can only be changed by editing the program. These parameters are printed on all hard copies of the results. After the documentation is entered, the program requests the scan parameters: scan rate (amu/s), sampling rate (points/s), the upper and lower masses (520-560), and the number of times the spectrum is to be scanned. With the first three, the equation in line 570 calculates the number of points/amu and the resulting total number of points to be taken over the amu range. The sampling rate divided by the scan rate gives the points/amu; subsequent multiplication by the amu range (upper mass minus lower mass) gives the total number of points in the scan. The total number of points establishes the iterations of the scan loop and the size of the array in which the data will be stored. For example, using a scan rate of 0.5 amu/s and a sampling rate of 10 points/s means that a point would be taken every 0.05 amu yielding 20 points/amu. Scanning over a range of 10 amu gives a total of 200 points in the

scan. After printing the calculated number of points, the program initializes all array locations to zero (590-610) and then begins the scan(s).

The scan loop (620-890) uses two external subroutines provided by the IBM Series 9000, SYSFUNC and AIN, written for controlling interfaced instruments and collecting data via an analog-to-digital (A/D) converter, respectively. A scan proceeds as follows. First, the A/D converter is opened as a file to read in data (the intensities in approximate microvolts). Next, with the subroutine's parameters, provided by the array FPK%(n), both external subroutines are called and initialized. The SYSFUNC subroutine resets the instrument to the lower mass to begin a scan by sending then terminating a +5-volt signal to the MS (740-800). Once reset, the AIN subroutine collects data (820-840) according to the parameters entered under command 1 of the menu. As the data are collected, intensities of corresponding amu are summed (860) for later averaging (930). Immediately following the scan, P_{MS} is read by the computer taking 30 readings (again using AIN) which are then averaged and placed in the appropriate array location for later observation, calculation, and storage (950-1020).

After collecting the raw data, the program extracts the detectable peaks and their intensities. Interfering raw data which might be interpreted as real peaks, such

as voltage spikes or out-of-range peaks (any intensity beyond the limits of the A/D converter, +/-1 V), are removed (1080-1210). This interfering data is removed using a simple loop which compares the read intensities to the limits of the A/D converter. With the false peaks removed, the program next identifies and prints the real peaks on the CRT (1220-1600).

Peaks are located by a method similar to a first derivative plot; or more simply where $dI_i/d(amu) = 0$, there is a peak. But d(amu) is a constant determined from the scan parameters that the user enters (generally 1 point/0.05 amu), so the derivatives need not be calculated. Instead, the intensities are compared. Where the differences in simultaneous intensities, dI_i, change from positive to negative, a peak exists. Using a loop and a logical AND statement, dI_i are calculated and compared (1270-1390). Upon meeting the requirements of the logical AND, the peak amu and intensity are determined. A loop within the one above (1330-1350) calculates the variance among the scans of a particular amu for further calculation of the standard deviation (1360).

Once the real peaks from a spectrum have been located, they are listed numerically from low amu to high on the CRT (1400-1440). Next, the operator has the choice of saving one or more of the listed peaks or

scanning a user-entered amu range again (1450-1460). Scanning again allows the intensity of a peak to be measured a second time or the intensity of a different peak at the same P_1 to be measured. On the other hand, if the user decides to save a peak, the desired peak is chosen from the list by entering the number preceding it (1480). The chosen peak is then saved in one of the preassigned data arrays, PK1(n)-PK5(n), by entering the number of the array, 1-5, to which the peak's amu value has been assigned earlier in the program (1470). The array location, n, is the present value of the point counter R. When several particular peaks in a spectrum are of interest, each can be scanned, chosen, and placed in its array one-at-a-time. This allows the intensities of several peaks in the spectrum at a given P_1 to be extracted individually without scanning an unwanted region of the spectrum between peaks separated by large amu difference. Instead, an entire spectral scan would be required, thus saving time, especially when a peak is scanned multiple times and averaged for one intensity determination.

With the peaks saved in the data arrays, the subroutine AIN reads the upstream P_1 and downstream P_2 pressures taking thirty measurements of each and averaging them. Next the subroutine corrects the already read P_{MS} for the kind of gas or gas mixture being tested and

for the scale range, 10^{-8}-10^{-5} torr, on which the analog display is presently located (1790-1909). Finally, G is requested and entered by the operator (1910), and then control is returned to the menu (1920).

It should be noted that all of the above information is for one point: one or more intensity measurements for the desired amu(s) at a given P_1. The array location of the measurements (I, G, P_2, etc.) associated with each operator-set P_1 is established by the point counter, R, (1630). Also, because commands 2 and 3 work in conjunction with this scanning subroutine it should be noted that command 2 in the menu allows scanning of the spectrum without changing any scan parameters, and command 3 allows just the upper and lower masses to be changed without changing any other scan parameters. These tasks are simply accomplished by passing-control from the menu to the scan subroutine at a location after the documentation and other scan parameters have been entered.

Data Observation

Commands 4-7 are designed to observe data and to decide whether or not the latest point or points are following certain trends as the P_1 is incremented during the experimental run. This enables the operator to determine whether possible spurious instrument or computer behavior has resulted in an invalid point. With

this information available after each point is taken, the operator can locate and correct any reasonable malfunctions and then repeat the point measurements without having to repeat the entire experimental run.

Command 4 allows the raw data, the actual computer-read intensities at each fractional amu, to be printed at the CRT. This is accomplished with a simple loop (1930-1980). Anomalous intensities (i.e. voltage spikes) or solely background readings suggest a problem either with the A/D converter or the MS.

Command 5 provides a CRT listing of the points from existing data or from an old data file called up for checking, calculation, or completion. (See Figure 8.) Formatted output and loops (size controlled by the point counter R) are used to accomplish this (1990-2190). Two tables are provided. The first table provides the latest R points in lists according to increasing pressure and includes the flow, pressures, and intensities for each amu scanned. The second table includes lists of ratios of intensities according to increasing P_1. Any errors in pressure or flow readings by the computer or operator would become evident here and could be corrected. There are two ways to correct pressure measurements: by repeating the entire point or by choosing peaks from the latest scan a second time (menu command 6). After listing the tables, the program asks the user if the

Figure 8. Representation of a typical CRT listing of data which can be seen using command 5 in the main menu.

DATE: 10/20/XX SAMPLE: 9.71% Ne, 9.77% Kr in N2
CONDITIONS: Straight-through Setup
FILE: 2:NKN2P50.DAT
MICROCHANNEL PLATE CODE: NONE
MASK CODE 50u
EMMISION CURRENT: 1.80 mA
IONIZATION POTENTIAL: 70.0 eV
MULTIPLIER SENSITIVITY: -1.00 kV
NUMBER OF SCANS AVERAGED 10

FLOW SCCM	P1 um	P2 um	PMS 1000um	I 14 mV	I 20 mV	I 42 mV	I 84 mV
0.00	12.3	9.3	0.157	3.86	0.00	5.69	3.66
0.01	15.9	9.3	0.288	8.98	3.44	6.15	7.74
0.02	18.5	9.3	0.354	12.26	4.71	6.59	11.30
0.03	24.5	9.4	0.507	19.95	7.45	8.15	18.60
0.06	31.4	9.7	0.680	28.27	10.64	9.99	25.73
0.11	45.0	10.1	1.012	43.53	16.70	13.13	37.16
0.16	61.0	10.6	1.419	57.18	23.24	16.38	48.10
0.29	91.5	11.4	2.131	89.77	36.38	22.29	68.24
0.51	136.4	13.0	3.133	130.71	54.79	30.84	95.31
0.83	188.3	14.1	4.264	177.27	73.17	36.01	120.78
1.36	258.4	15.9	5.810	236.03	99.83	50.78	161.11
1.86	314.9	17.5	7.023	282.74	118.55	60.69	193.63
2.79	402.2	19.7	8.818	346.51	148.10	75.95	239.65
3.68	473.9	22.0	10.295	387.33	171.41	88.01	268.58

P1/um	I84/I20	I84/I14	I20/I14	I42/I84
12.33	+.++++	0.9494	0.0000	1.5533
15.87	2.2482	0.8614	0.3832	0.7950
18.50	2.3990	0.9223	0.3845	0.5832
24.50	2.4984	0.9327	0.3733	0.4383
31.37	2.4174	0.9102	0.3765	0.3880
44.95	2.2251	0.8536	0.3836	0.3535
60.99	2.0693	0.8412	0.4065	0.3406
91.48	1.8758	0.7601	0.4052	0.3267
136.44	1.7397	0.7292	0.4191	0.3235
188.27	1.6506	0.6813	0.4128	0.2982
258.37	1.6138	0.6826	0.4229	0.3152
314.94	1.6332	0.6848	0.4193	0.3135
402.15	1.6182	0.6916	0.4274	0.3169
473.94	1.5669	0.6934	0.4425	0.3277

latest point is to be deleted (2170). If Y for yes is entered, the point counter R is held constant while the next point measurements are made and written over or placed in the array location of the spurious point. Corrections by the latter method are accomplished by choosing menu command 6 which passes control back to the listing of the major peaks (1400) allowing the same peak(s) to be relisted and saved as chosen originally and the pressure and flow measurements to be repeated, thus correcting them without repeating the scan. Command 6 also allows the user to reselect peaks from the latest scan if the wrong one was chosen from the list without repeating the scan. Again, control is returned to the menu upon completion of the function.

Graphing Subroutine

The most valuable means of observing the data to determine whether instrument or computer malfunction has occurred is graphically. A spurious point becomes evident when a trend established by a series of points is violated. When instrument and computer malfunction can be ruled out, such spurious points are easily corrected by taking another point under the same conditions and then comparing the two points graphically. Both points can be kept or rejected using the feature in command 5 of the menu discussed above which allows the latest point to be deleted.

Command 7 provides a plot of intensities, sensitivities (intensity/pressure), or ratios of intensities as a function of any of the three pressures, P_1, P_2, or P_{MS}. The operator need only enter the independent and dependent variables. Values normally left to the operator to enter are determined by the program from the chosen variables thus reducing the time required to view the graph.

The subroutine proceeds as follows. First, ON (variable) GOTO statements are used to place the operator chosen independent and dependent variables into the arrays IV(n) and DV(n), respectively, used during the rest of the subroutine (2200-2750). These generic arrays generalize the graphics treatment of the data allowing fewer program lines to plot more kinds of data. Next, the program locates the maximum and minimum values of the dependent variable using a basic sorting routine (2760-2870). The maximum and minimum values of the independent variable (a pressure) are simply the latest and the first value in the chosen pressure array as the pressure is incremented during the run. Using the maxima and minima, the axes' dimensions and tick mark increments (always ten), are calculated (2880-2920), and the screen is cleared for plotting (2930).

With the axes' dimensions and tick mark increments calculated, the program employs the subroutines LINE,

TEXT, and ELLIPSE within the graphics mode of the IBM 9000 (external to the main program) to draw axes and plot points. The graphics mode is invoked as a file would be using an OPEN FILE statement (2940). In general, LINE draws lines, TEXT writes alphanumeric characters, and ELLIPSE draws points each according to location, size, and orientation parameters provided by the calling program. Using the calculated values mentioned earlier, loops are established which use LINE to draw the axes and the tick marks and TEXT to write the associated numerical values (2950-3160). Finally, a similar loop employing LINE and ELLIPSE plots the data point by point (3170-3220).

Some additional features of the graphing subroutine are worth noting. The independent variable can be made to generate a logarithmic axis accomplished with a simple loop converting the values to logarithmic ones (2710-2750). Furthermore, the graphing subroutine can be called upon at any time between points to determine when point replications are necessary. This is a valuable timesaver because entire experimental runs are not necessary to confirm or reject spurious points.

Pertinent Calculations

Of immediate interest upon completion of an experimental run is the calculation of sensitivities as a function of pressure. The sensitivity of a given species

i, S_i, is defined by the equation

$$S_i = I_i/(X_i \cdot P_T) \qquad (7)$$

where I_i and X_i are the intensity and mole fraction of species i, respectively, and P_T is the total pressure (P_1, P_2, or P_{ms}). Note the value in parenthesis in equation 7 is the partial pressure of species i. Command 9 provides a hard copy of the sensitivities of an amu of interest as a function of all three pressures (3350-3810). Figure 9 shows an example listing of the sensitivities calculated from the raw data shown in Figure 8. The amu for which S_i is to be calculated is chosen by entering the number of the array (1-5) to which the amu was assigned in the parameter set-up (menu command 1). The measured intensity is read into a generic array (for ease of printout), then the sensitivities as a function of each pressure are calculated. Control is then passed to the output loop which prints the calculated values to the printer (3720). The table provides an operator entered title and the intensities, pressures, and sensitivities of the chosen amu in order of increasing pressure.

Command 10 provides hard copies of the raw data and intensity ratios exactly as seen at the CRT provided by command 5. The programming is exactly the same as in

Figure 9. A typical hard copy of sensitivities calculated for Ne-20 from the data shown in Figure 8.

Sensitivities for Ne-20

I mV	P1 um	S(P1) mV/um	P2 um	S(P2) mV/um	PMS um	10^-3 S(PMS) mV/u
0.00	12.3	0.000	9.3	0.00	0.157	0.0
3.44	15.9	2.233	9.3	3.81	0.288	123.1
4.71	18.5	2.622	9.3	5.23	0.354	137.1
7.45	24.5	3.130	9.4	8.14	0.507	151.3
10.64	31.4	3.494	9.7	11.28	0.680	161.3
16.70	45.0	3.826	10.1	17.08	1.012	169.9
23.24	61.0	3.925	10.6	22.66	1.419	168.7
36.38	91.5	4.095	11.4	32.75	2.131	175.8
54.79	136.4	4.135	13.0	43.51	3.133	180.1
73.17	188.3	4.002	14.1	53.47	4.264	176.7
99.83	258.4	3.979	15.9	64.55	5.810	176.9
118.55	314.9	3.877	17.5	69.91	7.023	173.9
148.10	402.2	3.793	19.7	77.25	8.818	173.0
171.41	473.9	3.725	22.0	80.13	10.295	171.5

command 5 except that data is written to a file opened as the printer. In addition, a hard copy of the standard deviations of each intensity for each amu of interest is provided. These values were calculated in the scan subroutine and were discussed earlier. Again loops and formatted output are used to print this data. It should be noted that since 10 scans were averaged for each intensity measurement, the standard deviation provided is actually the 99% confidence level.

Data Storage

Command 8 writes data to a floppy or hard disc for permanent storage. As a separate command in the menu, points can be saved as they are taken or a few at a time to prevent loss of data by a computer malfunction or by an operator error resulting in expulsion from the program. Data files are identified by the file name given to them in the parameter set-up (menu command 1). A simple loop sized by the point counter executes this task (3250-3320).

Ion Gauge Zeroing

Command 11 provides a method for determining the zero pressure of the ion gauge in the MS. The control box for the ion gauge provides an analog output of 0-2 volts DC to the A/D converter. Because the zero reading on the scale at the control box is not exactly 0 volts, it was thought that subtracting out the pressure differ-

ence would be advantageous. The zeroing is accomplished by using AIN (discussed earlier) to read the potential of the ion gauge, once zeroed (4360). This value is converted to a pressure (4400) and then subtracted from the succeeding ion gauge measurements made during the experimental run (1010). Preliminary results showed that the zero potential was sufficiently close to zero to be negligible and that the MS pressure measurements were closer to the actual ion gauge readings without zeroing. Consequently, zeroing was discontinued.

Exiting

The program can be exited in one of two ways (provided program execution has not been accidentally terminated). After each function is carried out by the specific command chosen from the menu, control is passed to line 270 which allows the operator to continue or exit the program. Entering the letter E exits the program; pressing the return key continues program execution by rewriting the menu. Exiting can also be accomplished by entering command 12 in the menu. Either of the methods of exiting passes control in the program to line 4440 which asks the operator whether the data has been saved. Entering Y for yes allows the user to exit the program; entering N for no passes control to command 8 in the menu and the data is automatically stored. This reminder helps prevent loss of data.

Unwanted, accidental exits from the program resulting in a loss of data have been prevented as much as possible by using ON ERROR GOTO statements wherever applicable in the program. Among the more common paths for being "kicked" out of the program is through entering values which are inapplicable or out-of-range of the allowed values. For example, entering a 15 for a menu function where only the values 1-12 are valid would result in an ejection from the program. This problem is circumvented in line 260 with the statement ON ERROR GOTO 420. When any error occurs, control is passed to line 420 where recovery occurs. For the error discussed above (58 in the computer's code), control is passed back to line 260, where the ON ERROR GOTO statement is reset for other potential errors. In this way a minimum of time is lost in repeating experimental runs due to lost data.

RESULTS AND CALCULATIONS

Mass Discrimination Effects

As mentioned in the Experimental section, we want to account for mass discrimination effects created by the inlet and/or the apparatus so that correct species concentrations can be calculated. In order to observe such effects, we consider the following. The intensity of a peak for any given amu is proportional to the concentration of the species as it is present in the ion source of the MS, or

$$I_i = k_i[i] \tag{8}$$

where k_i is a constant accounting for the isotopic abundance and the ionization efficiency and of species i at a given ionization potential. For a mixture of gases, the ratio of intensities would be

$$I_i/I_j = K[i]/[j] \tag{9}$$

where $K = k_i/k_j$. With K known, the ratio of concentrations of i and j in the mass spectrometer could be calculated as a function of pressure and compared to the

known concentration ratio of mixture in the source stream. Any mass discrimination effects would become evident from this data. Values for K are, however, unknown.

To circumvent the need for calculation of K, we compare the intensity ratios of the mixture gas with those obtained from pure gas data. This is simply a calibration of the apparatus and instrument using the pure gases. The ratio I_i/I_j for pure gases is obtained by dividing I_i at a given upstream pressure P_1 by I_j at the same P_1. For the gas mixture, we would expect I_i/I_j to equal $[i]/[j]$ in the gas canister. Any difference between the two suggests that mass enrichment has occurred for one of the species in the mixture. Using the intensity ratios for both the pure and mixture gases and defining the enrichment ratio E' as the ratio of these intensity ratios, we have

$$E' = (I_i/I_j)_m/(I_i/I_j)_p = ([i]/[j])_m/([i]/[j])_p \quad (10)$$

where the subscripts m and p refer to the mixture and pure gas data, respectively. Assuming K depends only on the species and <u>not</u> on the presence of other components, K cancels in the far right side of equation 10. Because pure gases cannot demonstrate mass discrimination effects as there is only one species present, only differences in

flow behavior between species where the mass discrimination effects arise are observed. If E'>1, the mixture has been enriched in species i upon flowing through the apparatus at the given pressure. If E'<1 then enrichment in species j has occurred. And if E'=1 then no enrichment has occurred.

Points in the experimental apparatus at which mass discrimination may be occurring are (1) in the quartz tube leading to the MS ion source, (2) at the inlet, either MCP or pinhole masked MCP, or (3) in the source stream. Figures 10-15 summarize these results for the sample gas 9.71% Ne, 9.77% Kr in N_2. Figures 10-12 show data for the straight-through configuration (Figure 5) with masks only, masked MCP-025, and masked MCP-CB inlets, respectively. Figures 13-15 show the corresponding data for the flow-by configuration. Each graph is a plot of I_{Kr}/I_{Ne} versus P_1 for a given experimental setup and inlet type. Within each graph, the lines are labeled according to gas (Mix or Pure) and diameter of the mask in micrometers. Mix refers to the sample gas mentioned above.

A few trends are immediately evident in each of the graphs. First, at corresponding pressures in each graph, I_{Kr}/I_{Ne} is higher for the sample gas than for the pure gases suggesting an enrichment in Kr, the heavier specie, in the sample gas upon flowing through the sample inlet

Figure 10. Intensity ratios, I_{Kr}/I_{Ne}, for the straight-through configuration with the mask inlets of the given dimensions.

PIN-HOLES, ST-THRU

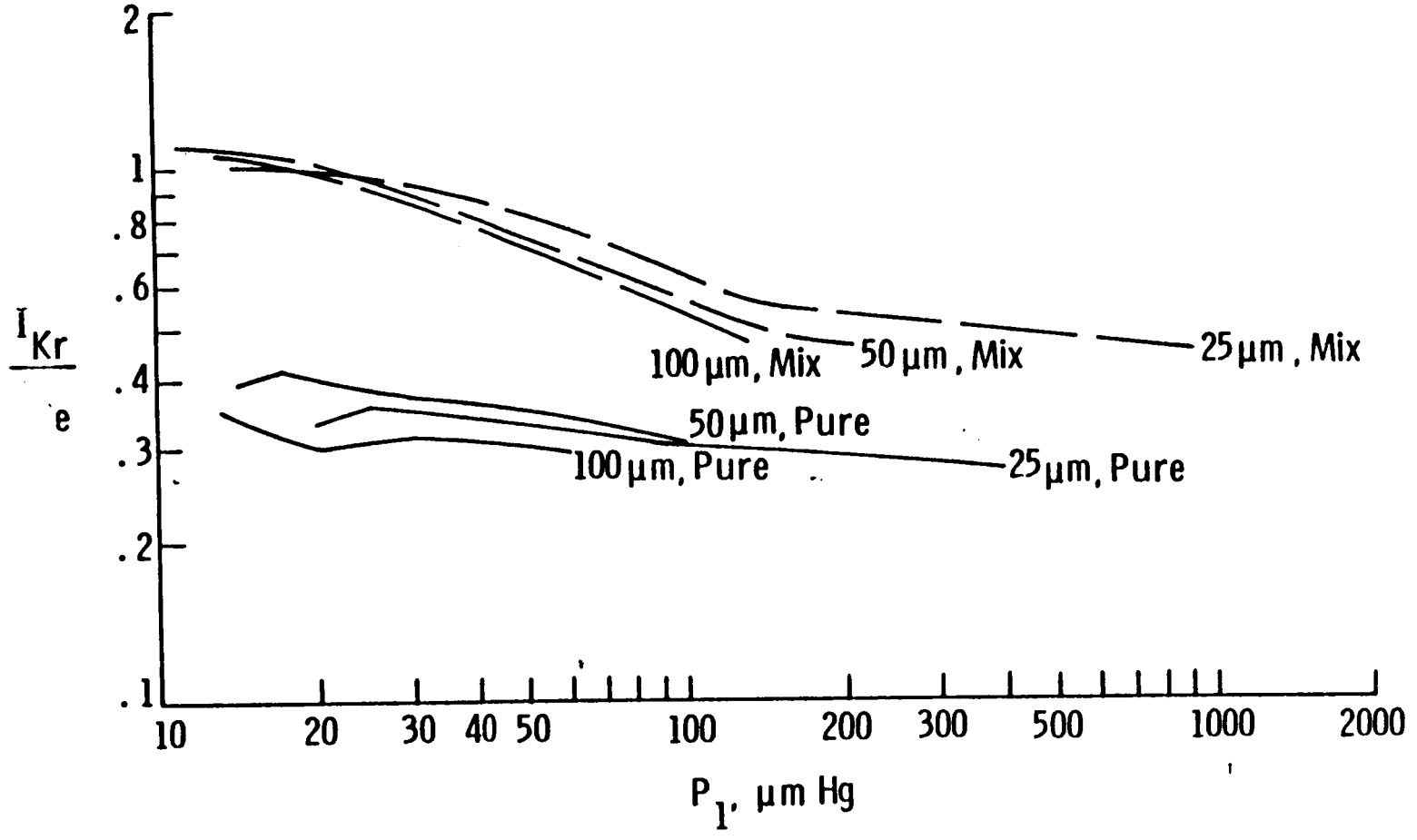

Figure 11. Intensity ratios, I_{Kr}/I_{Ne}, for the straight-through configuration with the masked MCP-025 inlet with varying mask dimensions.

MASKED MCP-025, ST-THRU

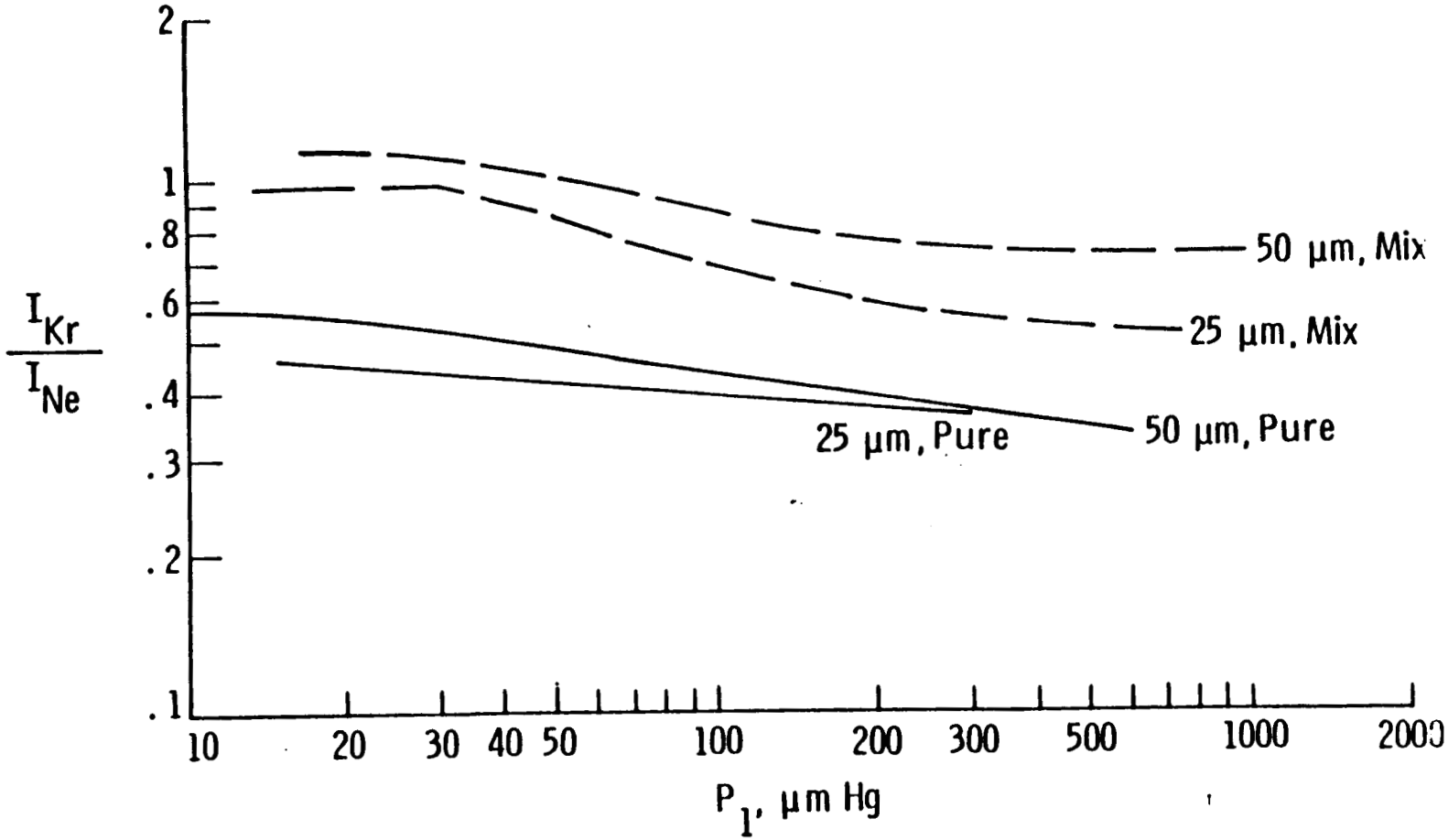

Figure 12. Intensity ratios, I_{Kr}/I_{Ne}, for the straight-through configuration with the masked MCP-CB inlet with varying mask dimensions.

MASKED MCP-CB, ST-THRU

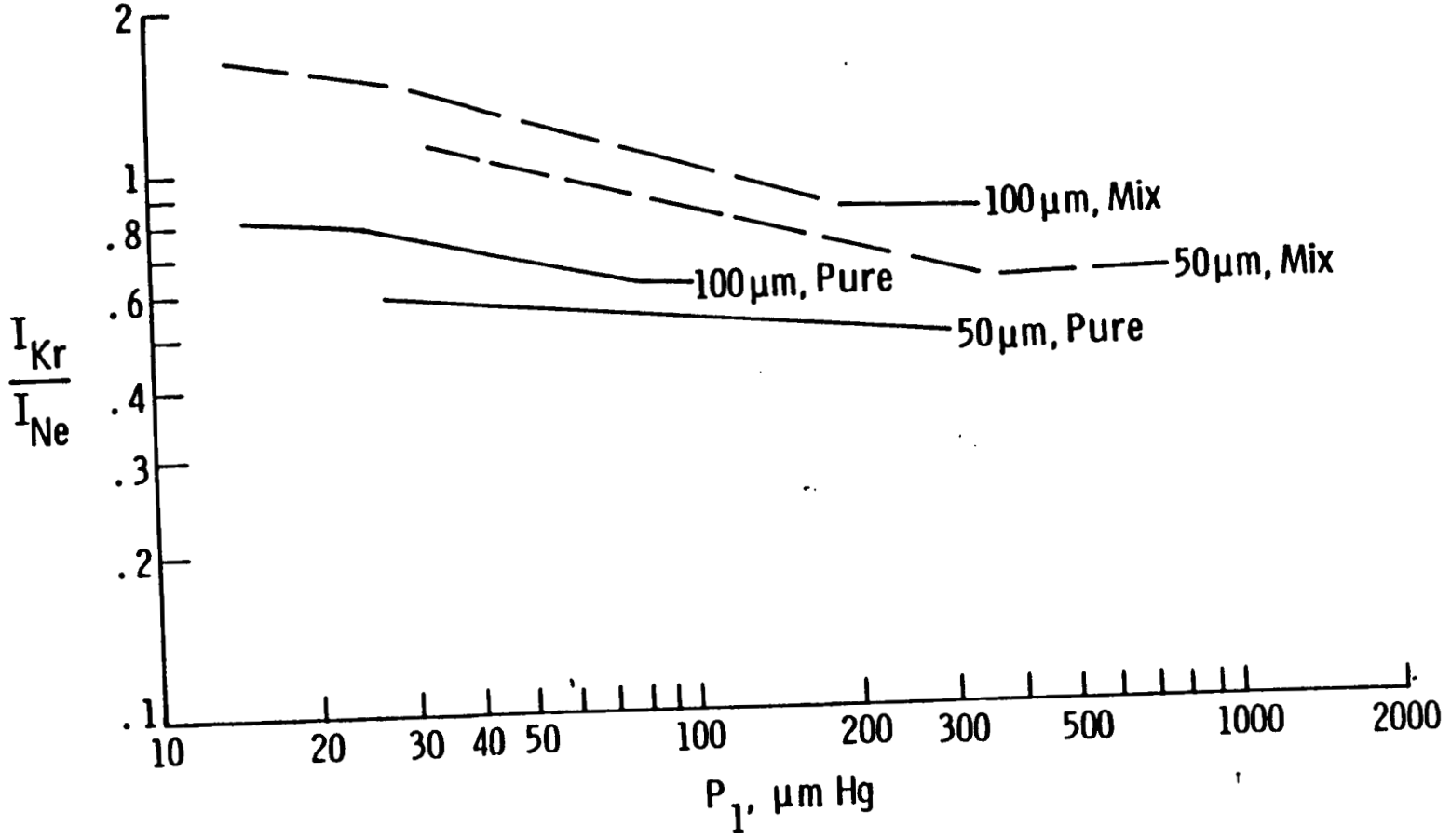

Figure 13. Intensity ratios, I_{Kr}/I_{Ne}, for the flow-by configuration with the mask inlets of the given dimensions.

PIN HOLES, FLOW-BY

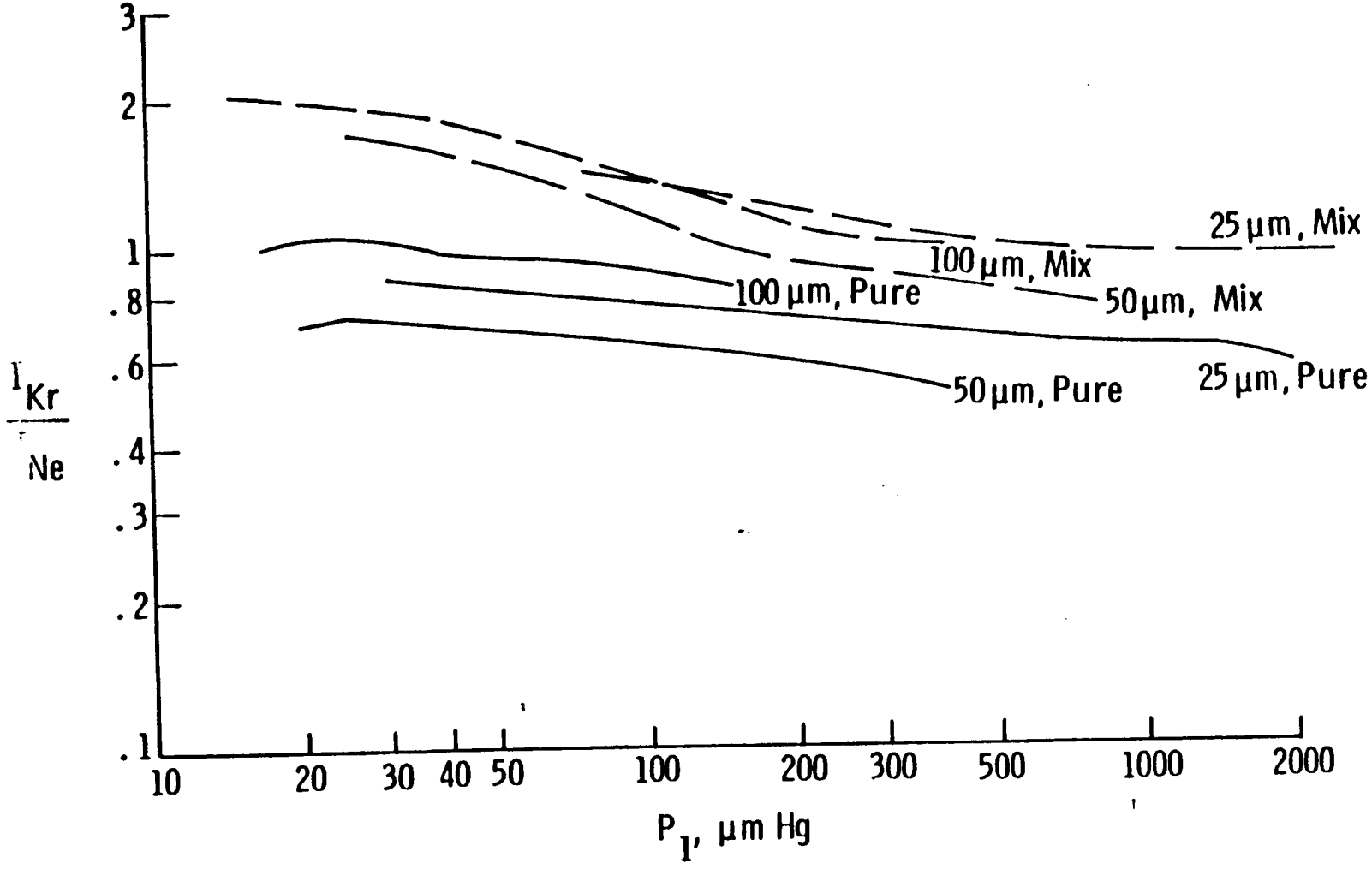

Figure 14. Intensity ratios, I_{Kr}/I_{Ne}, for the flow-by configuration with the masked MCP-025 inlet with varying mask dimensions.

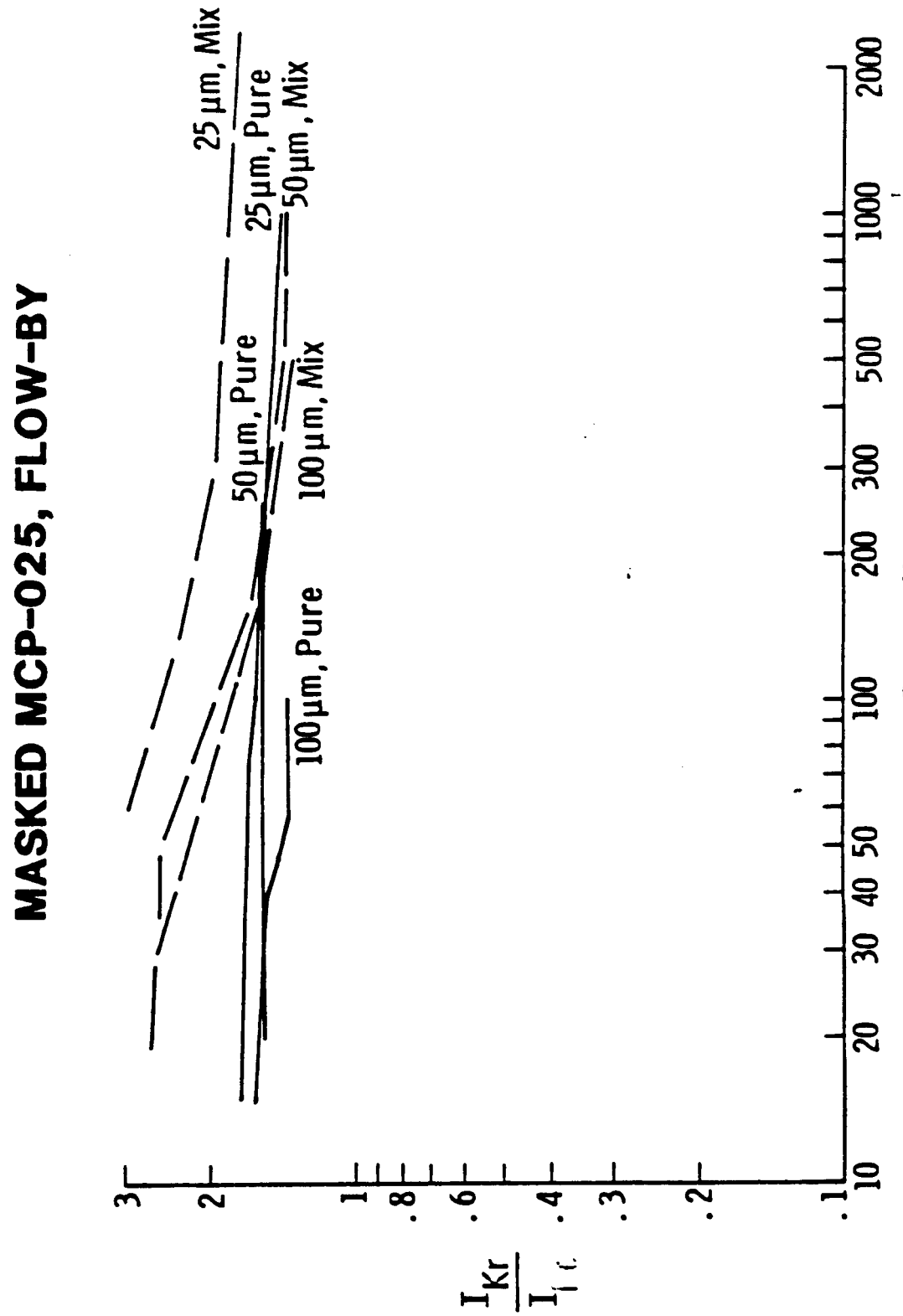
MASKED MCP-025, FLOW-BY
25 µm, Mix
25µm, Pure
50µm, Mix
50µm, Pure
100µm, Mix
100µm, Pure
3
2
1
.8
.6
.4
.3
.2
.1
10
20
30
40
50
100
200
300
500
1000
2000
P1, µm Hg

Figure 15. Intensity ratios, I_{Kr}/I_{Ne}, for the flow-by configuration with the masked MCP-CB inlet with varying mask dimension.

MASKED MCP-CB, FLOW-BY

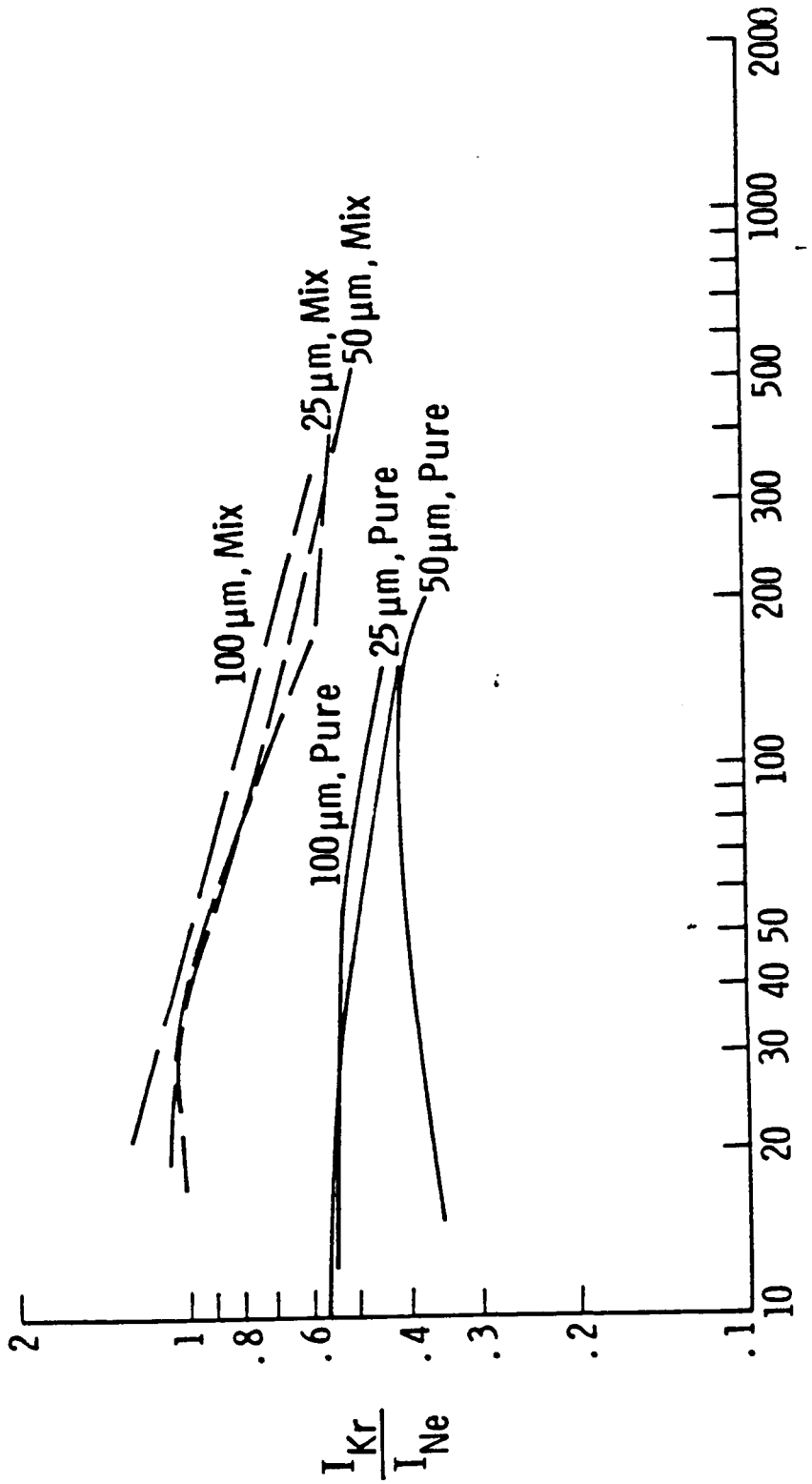

at any given pressure. Note this is contrary to the more frequently observed results for effusive flow, that is enrichment in the lighter species. Second, the enrichment in Kr is higher at lower pressures and gradually decreases as P_1 increases. This suggests that E' is approaching 1 because mixing occurs at higher pressures preventing mass discrimination. Third, comparing the flow-by data with the straight-through data, we see that the intensity ratios are, in general, higher in the former than in the latter, except for the ratios determined for MCP-CB which are approximately the same between the flow-by and straight-through configurations. And fourth, for both the pure gases and the sample gas, the resultant intensity ratios for the different mask inlets are in fairly good agreement with one another.

In addition, some expected trends which were not observed are worth noting. As the mask diameter varies, either as an inlet itself or as part of an MCP-mask inlet, intensity ratios vary randomly. For the straight-through configuration in Figure 10, for example, the data for the sample gas shows a slight increase in ratio over the pressure range as the mask inlet diameter decreases. For the pure gas data, however, the highest ratios are observed for the intermediate size mask (0.050 mm), and the ratios for the smallest mask (0.025 mm) are inter-

mediate; those for the 0.010 mm mask remain the smallest. Similar randomness is demonstrated by the data for other conditions. Because it is easy for some of the exposed capillaries to become clogged, however, it is difficult to ignore the trends existing in results as the mask size changes. Because the purpose of the masks as part of an MCP-mask combination is to cover the majority of the capillaries in the MCP, we might expect such randomness since it is the capillaries themselves and not the masks which should be responsible for creating effusive flow and the resulting mass discrimination effects.

Concentration Calculation

In order for the masked MCP to be useful as an inlet on the tethered satellite, it is necessary to account for the mass discrimination effects quantitatively. To the best of the author's knowledge, no literature exists which either qualitatively or quantitatively accounts for the behavior exhibited by our particular system. As a consequence, the concentrations of the species in a gas mixture are determined using calibration curves. The intensity of a species in a mixture or as a pure gas is directly proportional to its partial pressure in the MS; therefore, finding I_i as a funttion of pressure for a standard gas serves as a calibration of the apparatus for unknown mixtures. Because we want to known how the intensity varies with the source pressure, P_1 is the

pressure for which the apparatus is calibrated.

Preliminary results showed that I_i does not vary linearly with any of the measured pressures but, rather, shows a slight curvature. The reason for this nonlinearity is not fully understood, but it is believed to be caused by the transition from one flow regime to the next. As the flow regime changes, the amount of a species passing through the inlet may change giving some nonlinearity. As a result, the calibration curve is determined by fitting the intensity-pressure data with a second degree polynomial which provides a good fit showing, on the average, 3% deviation from the actual experimental points (see Figure 16). The resulting calibration curve is then

$$I_i = aP_{1,i}^2 + bP_{1,i} + c \qquad (11)$$

where $P_{1,i}$ is the partial pressure of species i and a, b, and c are fitting constants.

To determine the concentration of a species in a mixture the following procedure is followed: (1) intensity-pressure data are fitted with a second degree polynomial in $P_{1,i}$; (2) the resulting polynomial is solved for $P_{1,i}$ in terms of I_i using the quadratic formula

Figure 16. An example of a fitted calibration curve for ^{20}Ne, I_{Ne} versus P_1.

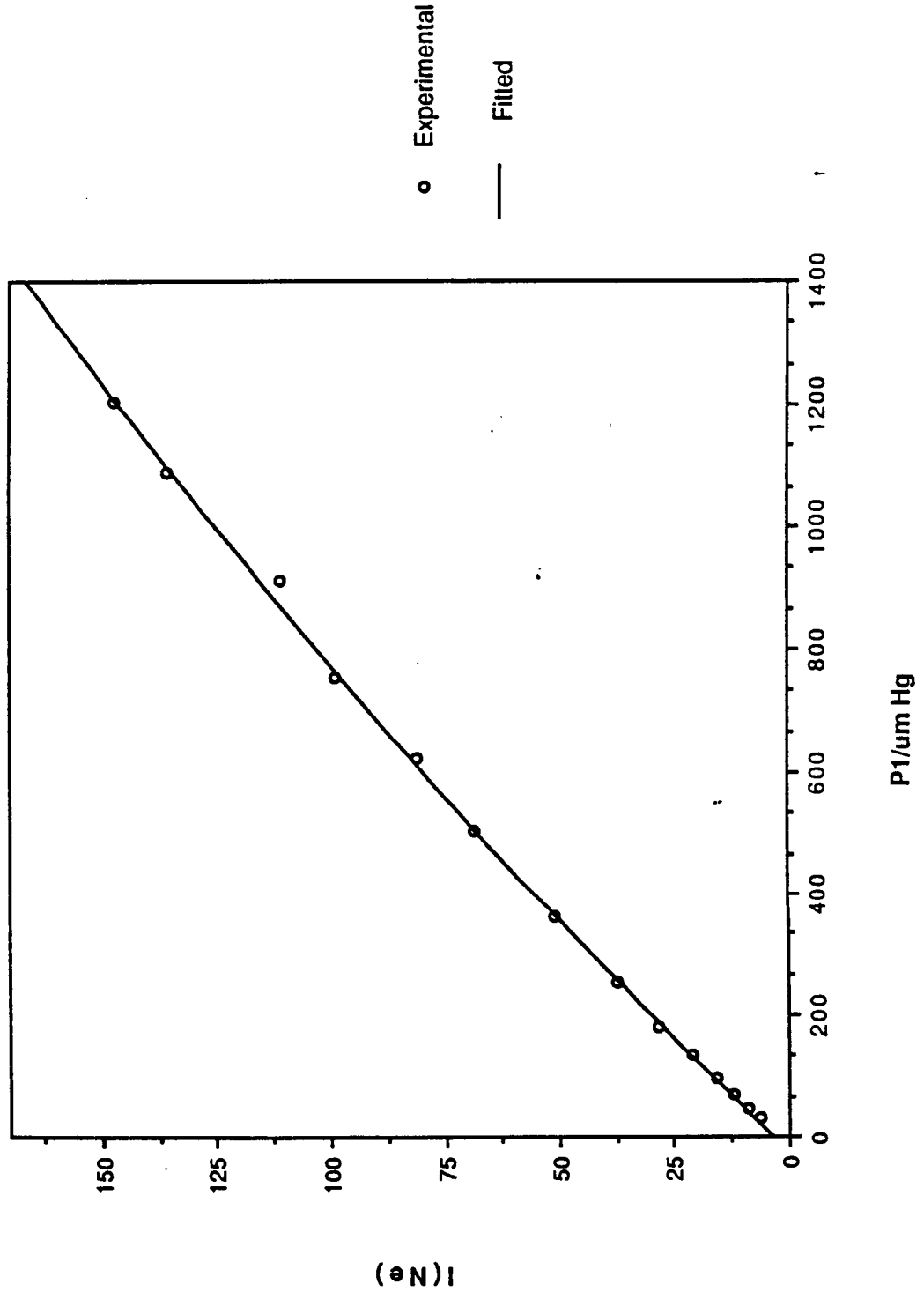
Experimental
Fitted
I(Ne)
150
125
100
75
50
25
0
0
200
400
600
800
1000
1200
1400
P1/um Hg

$$P_{1,i} = -b/2a \pm \sqrt{[(b^2-4a(c-I_i)]}/2a \qquad (12)$$

giving the partial upstream pressure of i in terms of intensity; and (3) intensity-pressure data from the sample gas are substituted into the appropriate calibration curve, equation 12, to calculate $P_{1,i}$ from which the mole fraction X_i in the source stream can be calculated using

$$X_i = P_{1,i}/P_{1,T} \qquad (13)$$

where $P_{1,T}$ is the total upstream pressure. It should be noted that the above method was accomplished using a computer program which used the stored data from the C-50 computer program. Also, the method was extended for use with P_2 and P_{MS}, but the results obtained using these pressures were more erratic and less accurate than those obtained from the upstream pressure data.

As with other applications, it is often better to calibrate the instrument using a standard mixture rather than pure gases to account for any interactive effects between gases. For our application, it is very possible that mixtures demonstrate different flow behaviors from the pure gases. As a result, a series of gases were tested for their appropriateness for calibration. These standard gases included pure, binary, and ternary

mixtures.

Table I shows the calculated mole fractions for a Ne-Kr-N_2 mixture for the straight-through configuration using the method described above. The first column in each table shows the total upstream pressure. The first column under each of the Neon and Krypton headings shows the measured mass spectral intensities from which the partial upstream pressures and resulting mole fractions were calculated using equations 11 and 12, respectively. The mixture composition was determined by GC to be 9.71% Ne and 9.77% Kr with the balance N_2. The standard gas, whose composition was also verified by GC, contained 5.08% Ne and 14.9% Kr with the balance N_2. The table below shows the fitting constants for the Ne and Kr calibration curves determined from the intensity-pressure data of the standard gas.

INLET	SPECIE	a	b	c
0.050-mm mask	Ne	-0.02627	4.297	1.572
	Kr	-0.02063	6.502	11.47
MCP-CB with 0.050-mm mask	Ne	-0.002119	1.598	2.477
	Kr	-0.001175	2.652	10.14

The calculated mole fractions are in reasonably good agreement with the expected values. It will be shown later that the majority of these values are within exper-

TABLE I. Calculated X(i) for sample gas containing 9.71% Ne and 9.77% Kr in N2 using standard containing 5.08% Ne and 14.9% Kr in N2 for given inlets

a. For 0.050-mm mask

Total P1	Neon			Krypton		
μm Hg	I/mV	P1/μm Hg	X	I/mV	P1/μm Hg	X
12.2	7.44	1.38	0.1133	14.94	0.53	0.0439
19.0	10.64	2.14	0.1123	22.07	1.64	0.0860
32.6	16.70	3.60	0.1103	33.50	3.42	0.1050
48.7	23.24	5.21	0.1070	44.43	5.15	0.1059
79.2	36.38	8.55	0.1080	64.58	8.39	0.1060
124.1	54.79	13.50	0.1087	91.65	12.85	0.1036
175.9	73.17	18.83	0.1070	117.11	17.18	0.0977
246.0	99.83	27.48	0.1117	157.44	24.33	0.0989
302.6	118.56	34.50	0.1140	189.96	30.38	0.1004
389.8	148.10	48.44	0.1243	235.98	39.47	0.1012
461.6	171.41	66.81	0.1477	264.92	45.56	0.0987

b. For 0.050-mm masked MCP-CB

Total P1	Neon			Krypton		
μm Hg	I/mV	P1/μm Hg	X	I/mV	P1/μm Hg	X
32.2	6.30	2.40	0.0749	15.11	1.88	0.0586
45.8	8.72	3.92	0.0857	19.17	3.41	0.0744
68.8	11.94	5.97	0.0866	25.95	5.98	0.0868
95.3	15.55	8.27	0.0868	32.54	8.48	0.0890
135.4	21.12	11.85	0.0875	42.33	12.20	0.0902
182.2	28.64	16.73	0.0918	54.30	16.77	0.0921
255.1	37.45	22.55	0.0884	72.26	23.67	0.0928
361.6	51.00	31.68	0.0876	99.59	34.24	0.0947
503.5	68.21	43.64	0.0867	133.13	47.36	0.0941
621.3	81.13	52.90	0.0851	160.30	58.11	0.0935
755.3	99.00	66.17	0.0876	195.39	72.15	0.0955
912.3	110.94	75.37	0.0826	229.71	86.07	0.0943
1088.9	135.60	95.30	0.0875	275.02	104.73	0.0962
1202.1	147.19	105.18	0.0875	114.57	114.57	0.0953

imental error only when the sample gas is used as a standard for itself.

Tables II and III summarize the mole fraction calculations for Ne and Kr based on various standard gases. It can be seen from these data that, as a whole, the pure gas standards provide poor estimates of the actual mole fractions of Ne and Kr in the tested gas. Because the binary and ternary standards more closely approximate this sample gas composition, it is understandable that calibrations derived from them would provide better results than those provided by the pure gas standards.

It is also instructive to note that the binary standards in some instances provide better results than the ternary standard where it might be expected that ternary should provide better results. This can be explained by considering the nearness of the compositions of these two standards. Both Ne and Kr are low relative to N_2 in both standards. In the ternary mixture, for example, both Ne and Kr encounter N_2 80% of the time. In the binary standard, both Ne and Kr encounter N_2 90% of the time. The nearness of the relative concentrations of Ne to N_2 and of Kr to N_2 in both standards would explain the nearness between the results obtained by these standards.

The last column in Tables II and III are calcula-

TABLE II. Summary of calculated X(i) for sample gas containing 9.71% Ne and 9.77% Kr in N2 using various standards for the 0.050-mm mask inlet

Total P1	Pure Ne and Kr		Ne-N2 and Kr-N2		5% Ne, 15% Kr in N2		10% Ne, 10% Kr in N2	
μm Hg	X(Ne)	X(Kr)	X(Ne)	X(Kr)	X(Ne)	X(Kr)	X(Ne)	X(Kr)
12.2	-0.1140	-0.0460	0.1013	0.0514	0.1133	0.0439	0.0919	0.0898
19.0	-0.0380	0.0112	0.1088	0.0885	0.1123	0.0860	0.0972	0.1104
32.6	0.0165	0.0447	0.1126	0.1040	0.1103	0.1050	0.0994	0.1147
48.7	0.0391	0.0545	0.1115	0.1037	0.1070	0.1059	0.0979	0.1096
79.2	0.0588	0.0615	0.1138	0.1026	0.1080	0.1060	0.0994	0.1052
124.1	0.0687	0.0635	0.1144	0.0994	0.1087	0.1036	0.0994	0.1007
175.9	0.0706	0.0610	0.1113	0.0932	0.1070	0.0977	0.0963	0.0942
246.0	0.0737	0.0623	0.1131	0.0935	0.1117	0.0989	0.0973	0.0953
302.6	0.0732	0.0631	0.1123	0.0943	0.1140	0.1004	0.0962	0.0971
389.8	0.0733	0.0630	0.1139	0.0941	0.1243	0.1012	0.0968	0.0990
461.6	0.0730	0.0607	0.1158	0.0911	0.1477	0.0987	0.0976	0.0976

TABLE III. Summary of calculated X(i) for sample gas containing 9.71% Ne and 9.77% Kr in N2 using various standards for the 0.050-mm masked MCP-CB inlet

Total P1	Pure Ne and Kr		Ne-N2 and Kr-N2		5% Ne, 15% Kr in N2		10% Ne, 10% Kr in N2	
μm Hg	X(Ne)	X(Kr)	X(Ne)	X(Kr)	X(Ne)	X(Kr)	X(Ne)	X(Kr)
32.2	-0.1104	-0.0395	0.1013	0.1189	0.0749	0.0586	0.0833	0.1017
45.8	-0.0385	0.0133	0.0747	0.1202	0.0857	0.0744	0.0959	0.1046
68.8	0.0087	0.0545	0.0859	0.1213	0.0866	0.0868	0.0974	0.1070
95.3	0.0341	0.0715	0.087	0.1166	0.0868	0.0890	0.0977	0.1036
135.4	0.0542	0.084	0.0871	0.1124	0.0875	0.0902	0.0987	0.1005
182.2	0.0707	0.0931	0.0878	0.1110	0.0918	0.0921	0.1036	0.0998
255.1	0.0760	0.0996	0.0919	0.1088	0.0884	0.0928	0.0998	0.0984
361.6	0.0814	0.1060	0.0881	0.1084	0.0876	0.0947	0.0988	0.0989
503.5	0.0839	0.1081	0.0868	0.1057	0.0867	0.0941	0.0977	0.0973
621.3	0.0835	0.1088	0.0851	0.1040	0.0851	0.0935	0.0959	0.0963
755.3	0.0865	0.1123	0.083	0.1050	0.0876	0.0955	0.0986	0.0981
912.3	0.0815	0.1117	0.0791	0.1027	0.0826	0.0943	0.0928	0.0967
1088.9	0.0856	0.1147	0.0823	0.1034	0.0875	0.0962	0.0981	0.0985
1202.1	0.0849	0.1140	0.0815	0.1019	0.0875	0.0953	0.0979	0.0976

tions for the sample gas using itself as a standard. This gives a good estimate of the error involved in the method and will be discussed later.

Results for the calculated mole fractions using 5.08% Ne and 14.9% Kr in N_2 as the sample gas and the others as standards can be found in Appendix B. Appendix B also has the results of the CO_2-air mixtures tested on the UTI experimental setup (Figure 6).

In summary, the calculated compositions, as a whole, are in reasonably good agreement with real compositions. Mole fractions obtained at the lowest P_1's are rarely in agreement with the real values. This is not fully understood but is believed to be caused by background gases adsorbed to the wall of the tubing leading from the gas canisters to the MS. It is also possible that some flow effects at the lowest pressures are involved. At increased pressures the results improve, and at the highest pressures, the results are generally in good agreement with the real values. Recall that as the pressure increases, mass discrimination effects become negligible suggesting that flow effects may be responsible for the poor values obtained at the lowest pressures.

The calculated mole fractions for Ne and Kr, summarized in Table II, are plotted as a function of P_1 in Figures 17 and 18, respectively. The sample gas is

Figure 17. X_{Ne} from the sample gas containing 9.71% Ne and 9.77% Kr in N_2 calculated from data on various standards for the 0.050-mm inlet on the straight-through setup.

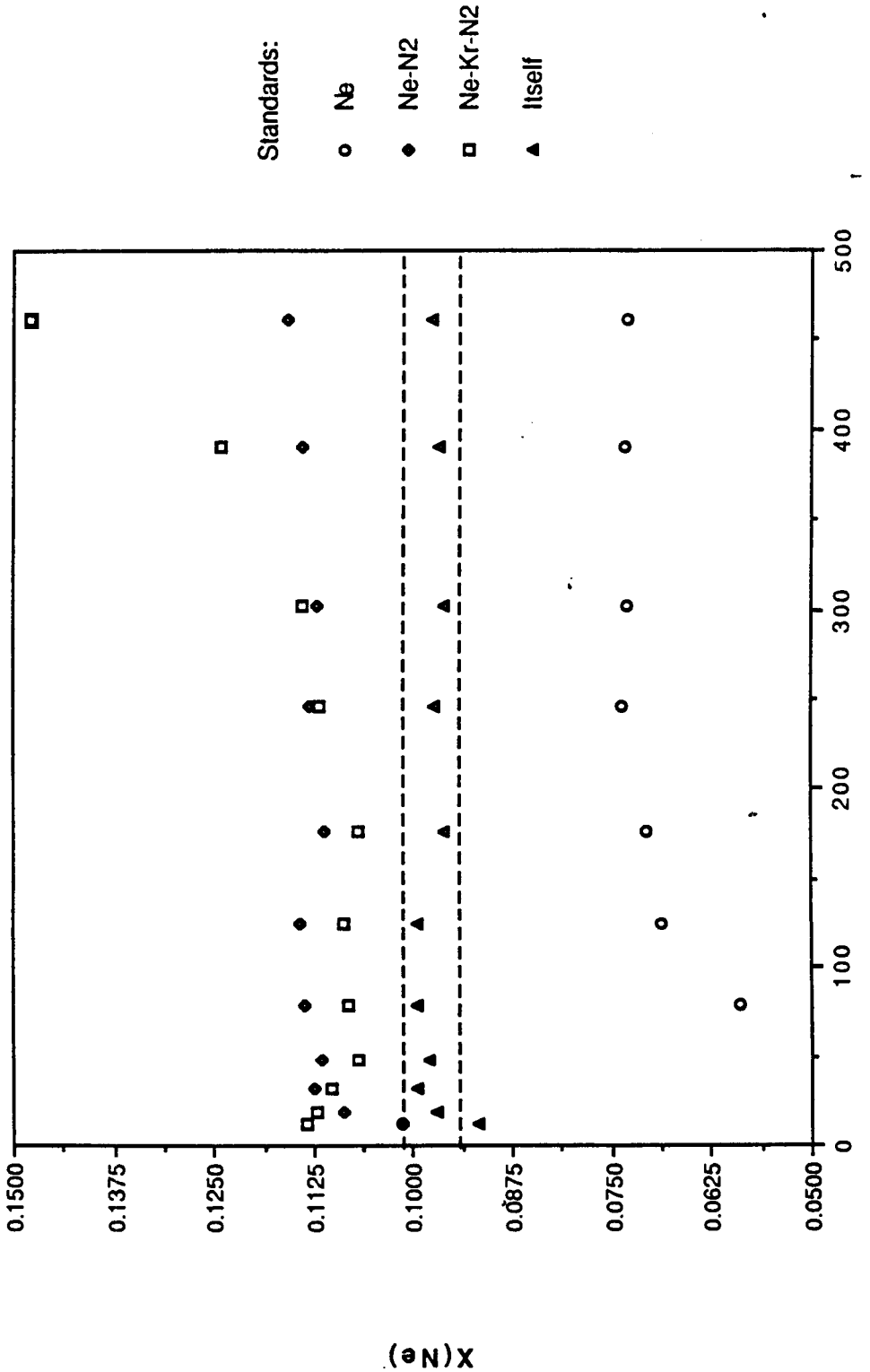
Standards:
Ne
Ne-N2
Ne-Kr-N2
Itself
0.1500
0.1375
0.1250
0.1125
0.1000
0.0875
0.0750
0.0625
0.0500
0
100
200
300
400
500
X(Ne)
P1/um Hg

Figure 18. X_{Kr} from the sample gas containing 9.71% Ne and 9.77% Kr in N_2 calculated from data on various standards for the 0.050-mm inlet on the straight-through setup.

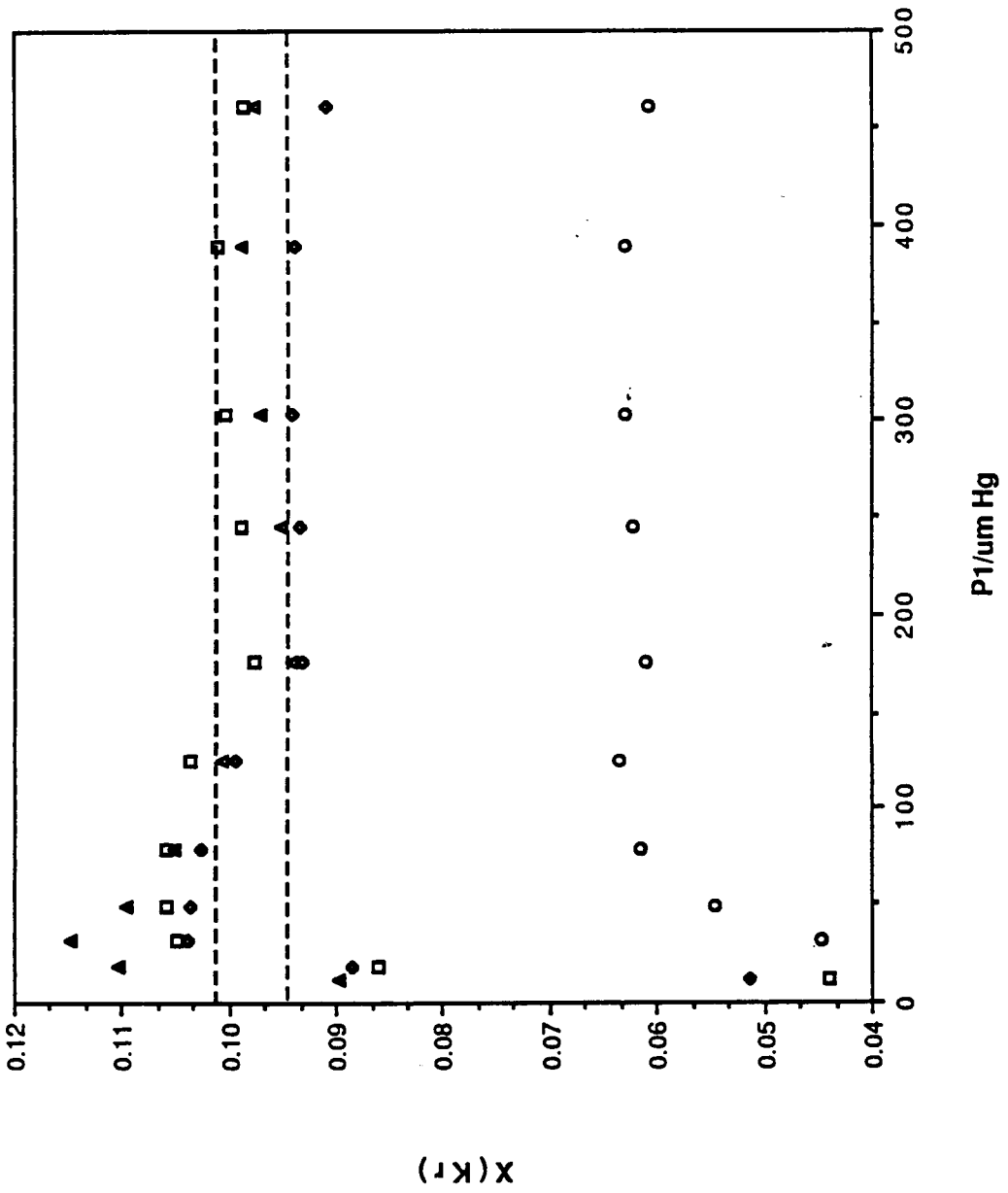
Standards:
Kr
Kr-N2
Ne-Kr-N2
Itself
X(Kr)
0.12
0.11
0.10
0.09
0.08
0.07
0.06
0.05
0.04
0
100
200
300
400
500
P1/um Hg

9.71% Ne and 9.77% Kr in N_2, and the inlet is the 0.050-mm mask. Based on the known percentages of Ne and Kr in the mixture, the expected values for X_{Ne} and X_{Kr} are 0.0971 and 0.0977, respectively. These graphs show that the pure gases are poor standards for the mixture gas, whereas the binary and ternary mixtures are better. The pure gas standards yield lower values than expected for both Ne and Kr. The binary and ternary standards give reasonably close results, but are not within the limits of error. When the sample gas itself is used as a standard, the calculated mole fractions are within the expected range of values except at the lowest pressures.

These graphs also make more evident the problem of determining accurate mole fractions at the lowest pressures. The difficulty in determining accurate mole fraction at the lowest pressures prompted the use of an alternative method for calculation of the mole fractions. The first several points of I_i versus P_1 for the majority of the data appeared to be linear. The curvature only became apparent as the pressure increased. This is reasonable because of transitions between flow regimes as the pressure increases. For this reason the data for the lowest pressures were considered separately fitting the I_i versus P_1 with a linear least-squares line for calibration. The resulting calculated mole fractions showed no significant difference from those obtained by

considering the data as a whole. This suggests that the method of calculation is not at fault in determining accurate mole fractions at the lowest pressures and supports the hypothesis of background gas affecting the calculated values.

Similar graphs of mole fraction versus P_1 for Ne and Kr for the same sample gas but for the 0.050-mm masked MCP-CB (summarized in Table III) are shown in Figures 19 and 20. The same trends are found for these data as was found for those just discussed with the exception that the pure Kr standard provided a higher than expected mole fraction rather than a lower. This suggests that the MCP portion of the inlet might be a factor in enriching the Kr. Compared to the binary and ternary standards which would show similar mass enrichment as the sample gas, the pure gas could not. As a result, an I_{Kr} from the sample gas data substituted into the pure Kr calibration equation for which no enrichment in Kr could be observed would yield a higher than expected partial pressure for Kr and a resulting higher than expected X_{Kr}.

Figures 21-24 show the same graphs as above except that the sample gas is 5.08% Ne and 14.9% Kr in N_2 and the other gases are used as standards. Again, the same trends are seen as for the sample gas shown in Figures 17-20. Note that, again, higher than expected values are obtained for X_{Kr} when the inlet is a MCP-mask combination

Figure 19. X_{Ne} from the sample gas containing 9.71% Ne and 9.77% Kr in N_2 calculated from data on various standards for the 0.050-mm masked MCP-CB inlet on the straight-through setup.

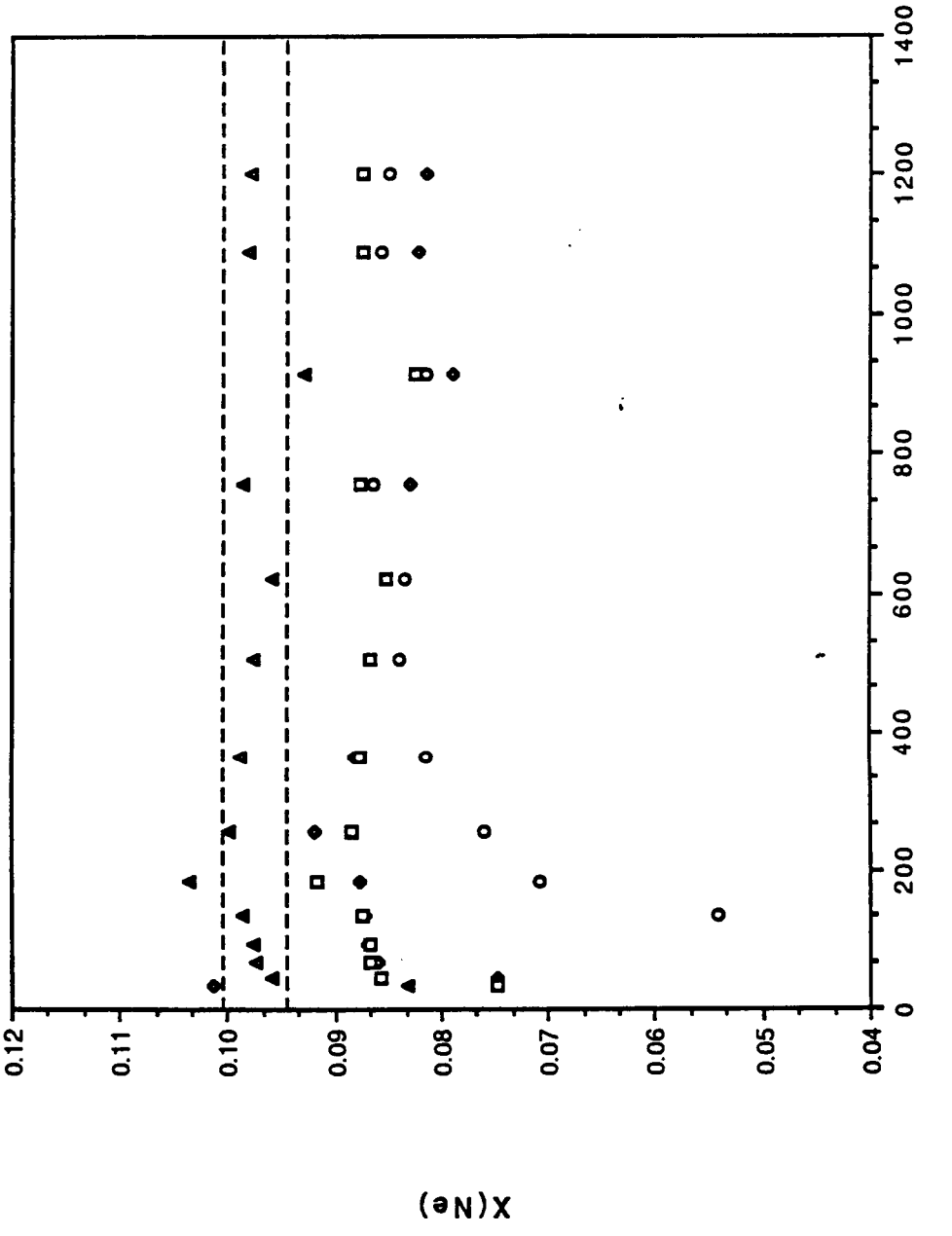
Standards:
Ne
Ne-N2
Ne-Kr-N2
Itself
X(Ne)
P1/ um Hg
0.12
0.11
0.10
0.09
0.08
0.07
0.06
0.05
0.04
0
200
400
600
800
1000
1200
1400

Figure 20. X_{Kr} from the sample gas containing 9.71% Ne and 9.77% Kr in N_2 calculated from data on various standards for the 0.050-mm masked MCP-CB inlet on the straight-through setup.

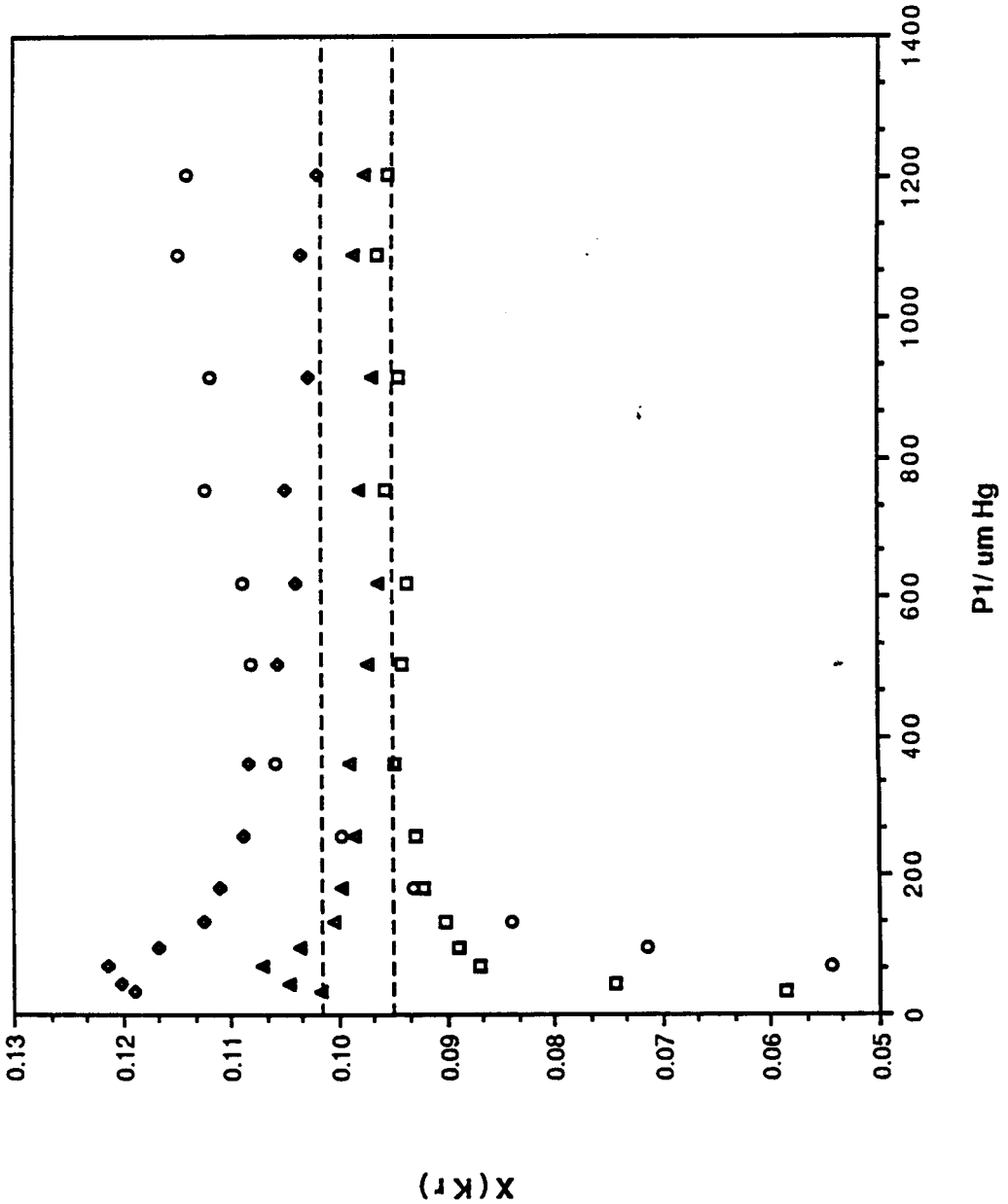
Standards:
Kr
Kr-N2
Ne-Kr-N2
Itself
0.13
0.12
0.11
0.10
0.09
0.08
0.07
0.06
0.05
0
200
400
600
800
1000
1200
1400
P1/ um Hg
X(Kr)

Figure 21. X_{Ne} from the sample gas containing 5.08% Ne and 14.9% Kr in N_2 calculated from data on various standards for the 0.050-mm inlet on the straight-through setup.

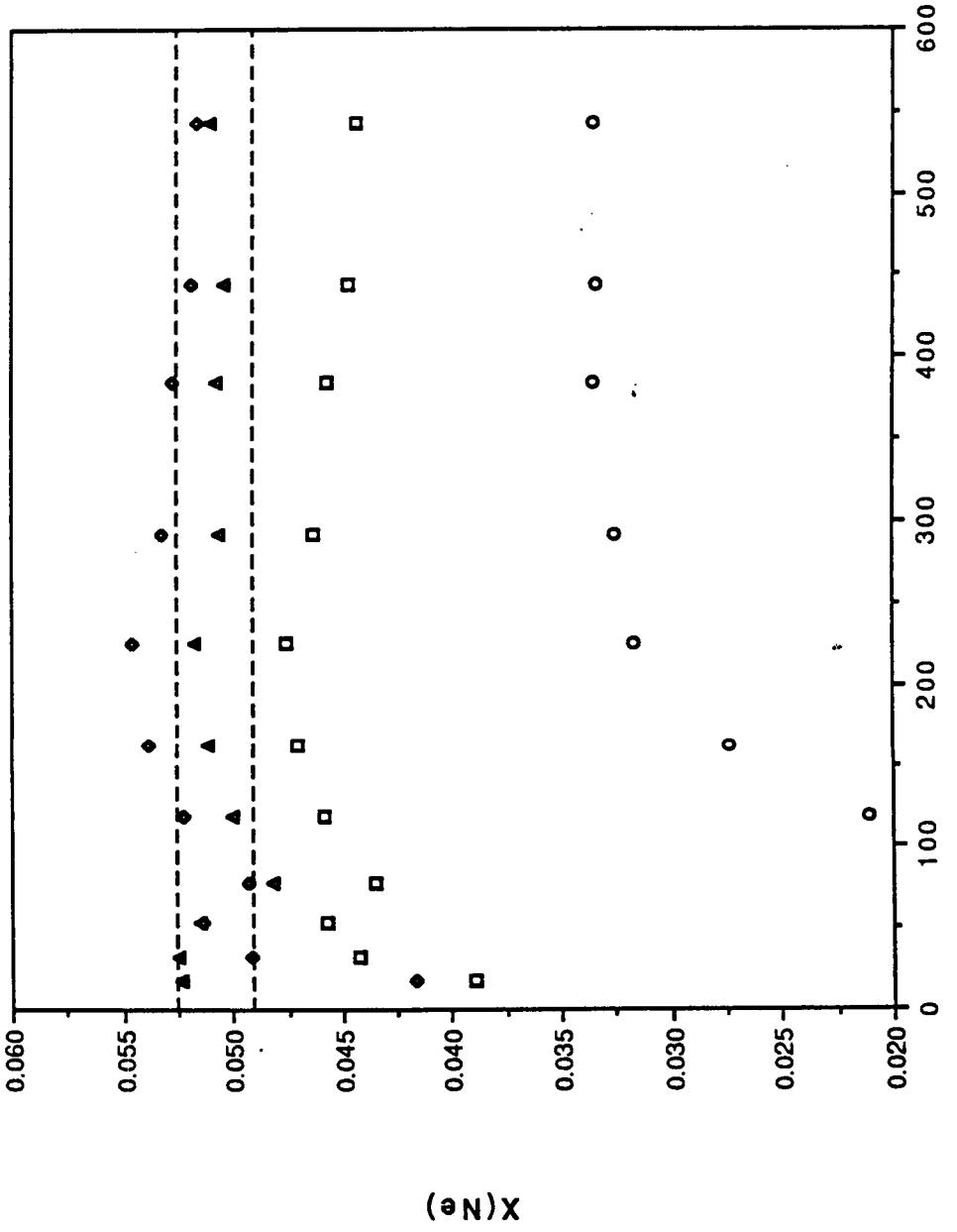
Standards:
Ne
Ne-N2
Ne-Kr-N2
Itself
X(Ne)
0.060
0.055
0.050
0.045
0.040
0.035
0.030
0.025
0.020
0
100
200
300
400
500
600
P1/um Hg

C-2

Figure 22. X_{Kr} from the sample gas containing 5.08% Ne and 14.9% Kr in N_2 calculated from data on various standards for the 0.050-mm inlet on the straight-through setup.

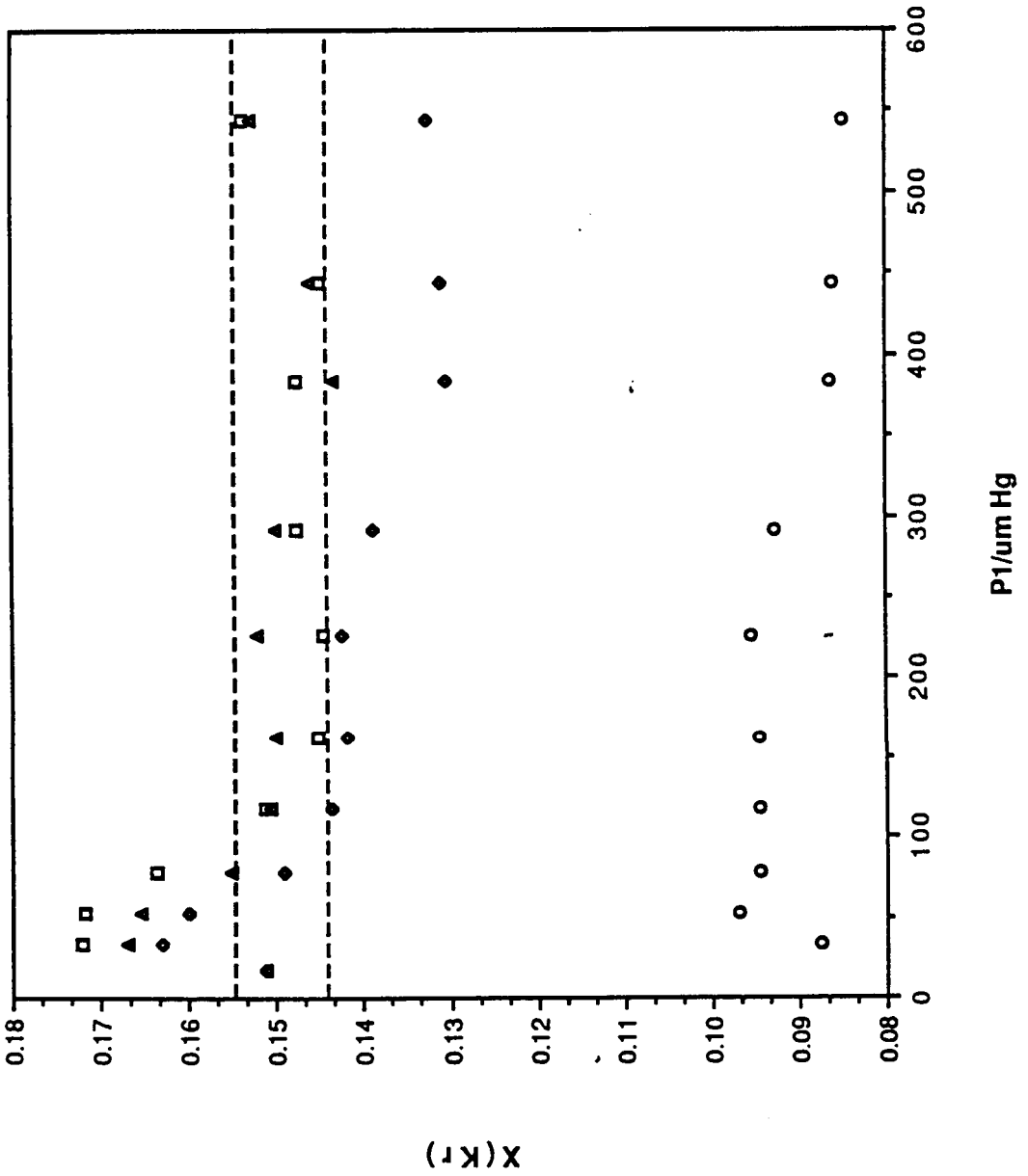
Standards:
Kr
Kr-N2
Ne-Kr-N2
Itself
X(Kr)
P1/um Hg
0.18
0.17
0.16
0.15
0.14
0.13
0.12
0.11
0.10
0.09
0.08
0
100
200
300
400
500
600

Figure 23. X_{Ne} from the sample gas containing 5.08% Ne and 14.9% Kr in N_2 calculated from data on various standards for the 0.050-mm masked MCP-CB inlet on the straight-through setup.

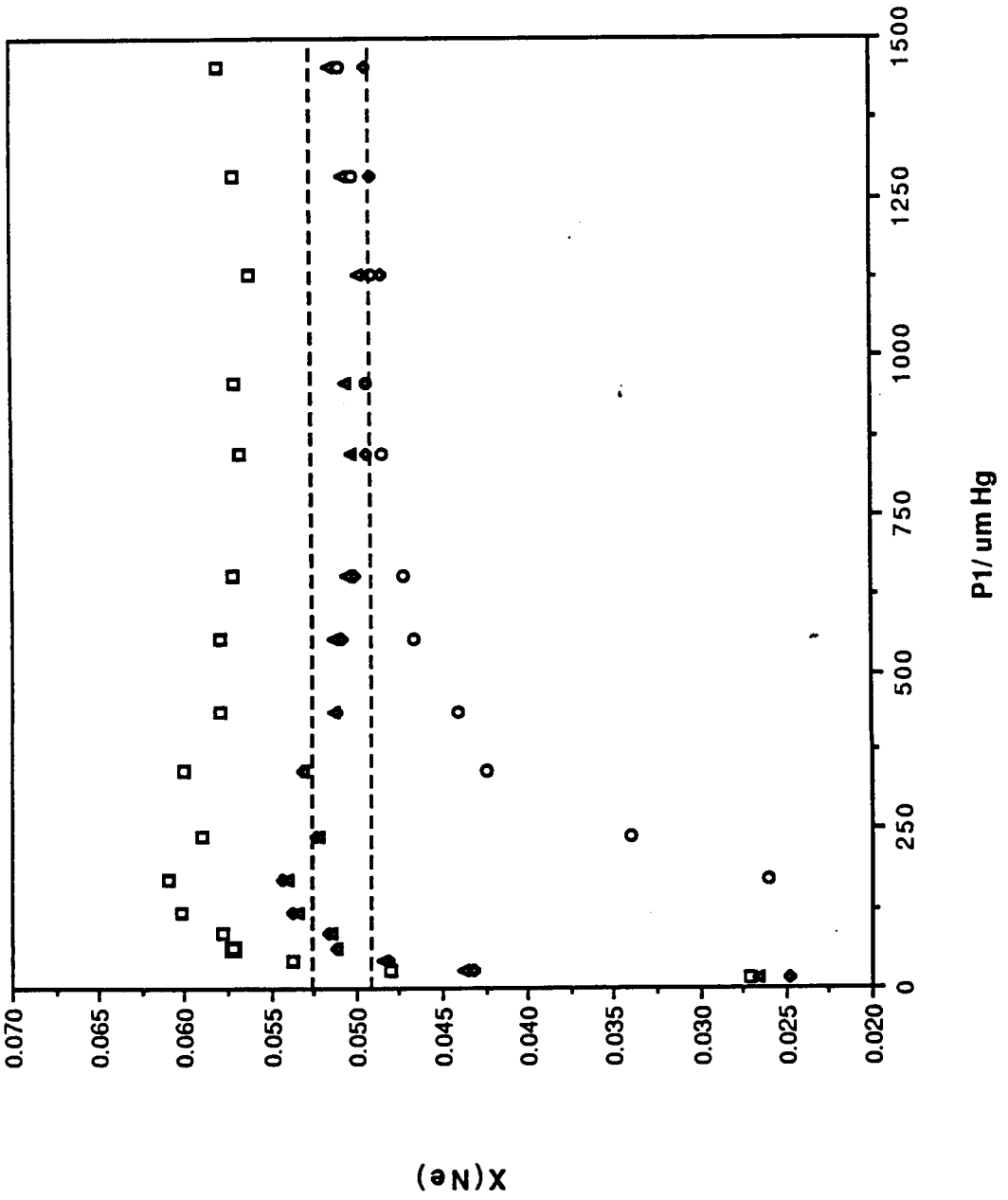
Standards:
Ne
Ne-N2
Ne-Kr-N2
Itself
X(Ne)
P1/ um Hg
0.070
0.065
0.060
0.055
0.050
0.045
0.040
0.035
0.030
0.025
0.020
0
250
500
750
1000
1250
1500

Figure 24. X_{Kr} from the sample gas containing 5.08% Ne and 14.9% Kr in N_2 calculated from data on various standards for the 0.050-mm masked MCP-CB inlet on the straight-through setup.

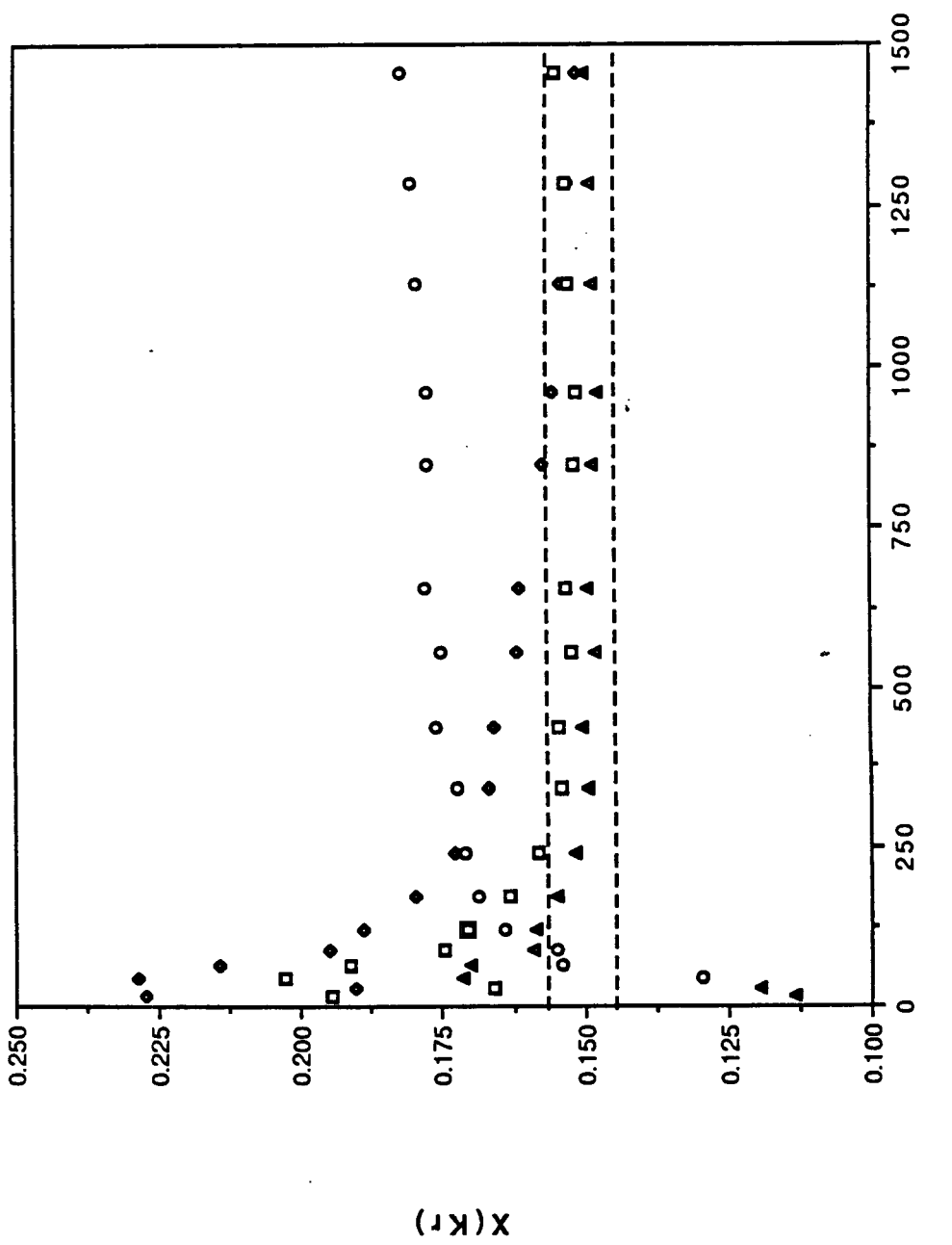
Standards:
Kr
Kr-N2
Ne-Kr-N2
Itself
X(Kr)
0.250
0.225
0.200
0.175
0.150
0.125
0.100
0
250
500
750
1000
1250
1500
P1/um Hg

and pure Kr is used as the standard gas. This supports the observation made above concerning the enrichment in Kr attributed to the MCP.

Figures 25-27 show similar graphs to the ones above, but the sample gases are the CO_2-air mixtures tested on the UTI experimental setup (Figure 6). Each of the CO_2-air mixtures provides the expected values for X_{CO2} and X_{O2} within error when each is used as a standard for itself as was observed for the Ne-Kr-N_2 mixtures. While each of the 7.55% CO_2-air and the 15.44% CO_2-air mixtures provide reasonably good mole fractions when used as a standard for the other, neither provided good results when used as a standard for the 3.033% CO_2-air mixture. Nor did the 3.033% CO_2-air mixture provide good results when used as a standard for the other two CO_2-air mixtures. This observation suggests that the flow behavior of the 3.033% CO_2-air mixture might be significantly different from the other two CO_2-air mixtures.

Error Analysis

Based on the method of calculation, two forms of uncertainty must be considered in order to determine the overall uncertainty in the calculated mole fractions: (1) the uncertainty in I_i for the sample gas and (2) the uncertainty in I_i for the standard gas used for calibration. If we consider the calibration curve to alleviate

Figure 25. X_{CO2} from the sample gas containing 7.55% CO_2 in air calculated from data on various standards for the 0.035-mm inlet on the UTI setup.

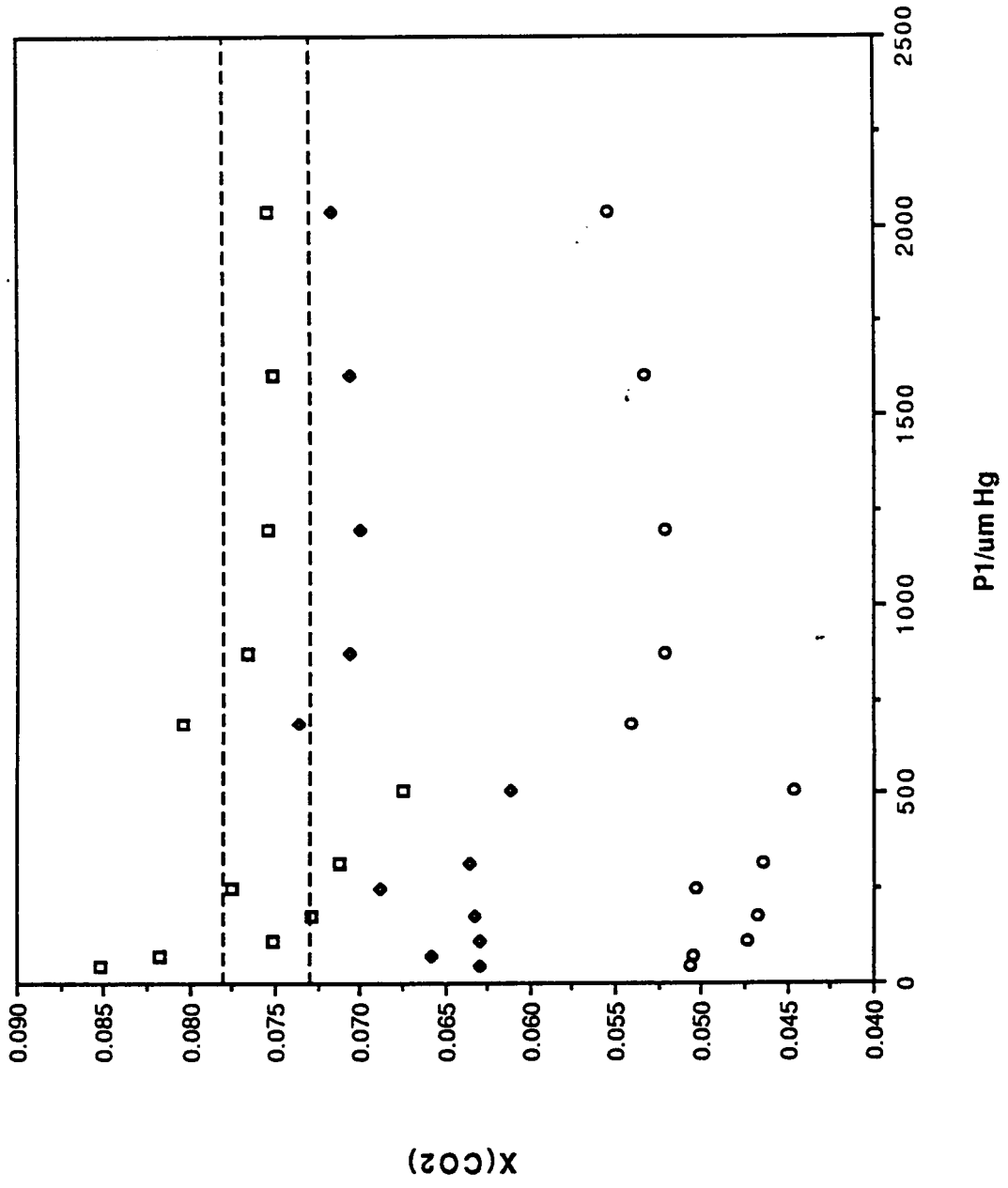
Standards:
3% CO2-air
15% CO2-air
Itself
x(CO2)
0.090
0.085
0.080
0.075
0.070
0.065
0.060
0.055
0.050
0.045
0.040
0
500
1000
1500
2000
2500
P1/um Hg

Figure 26. X_{CO2} from the sample gas containing 15.44% CO_2 in air calculated from data on various standards for the 0.035-mm inlet on the UTI setup.

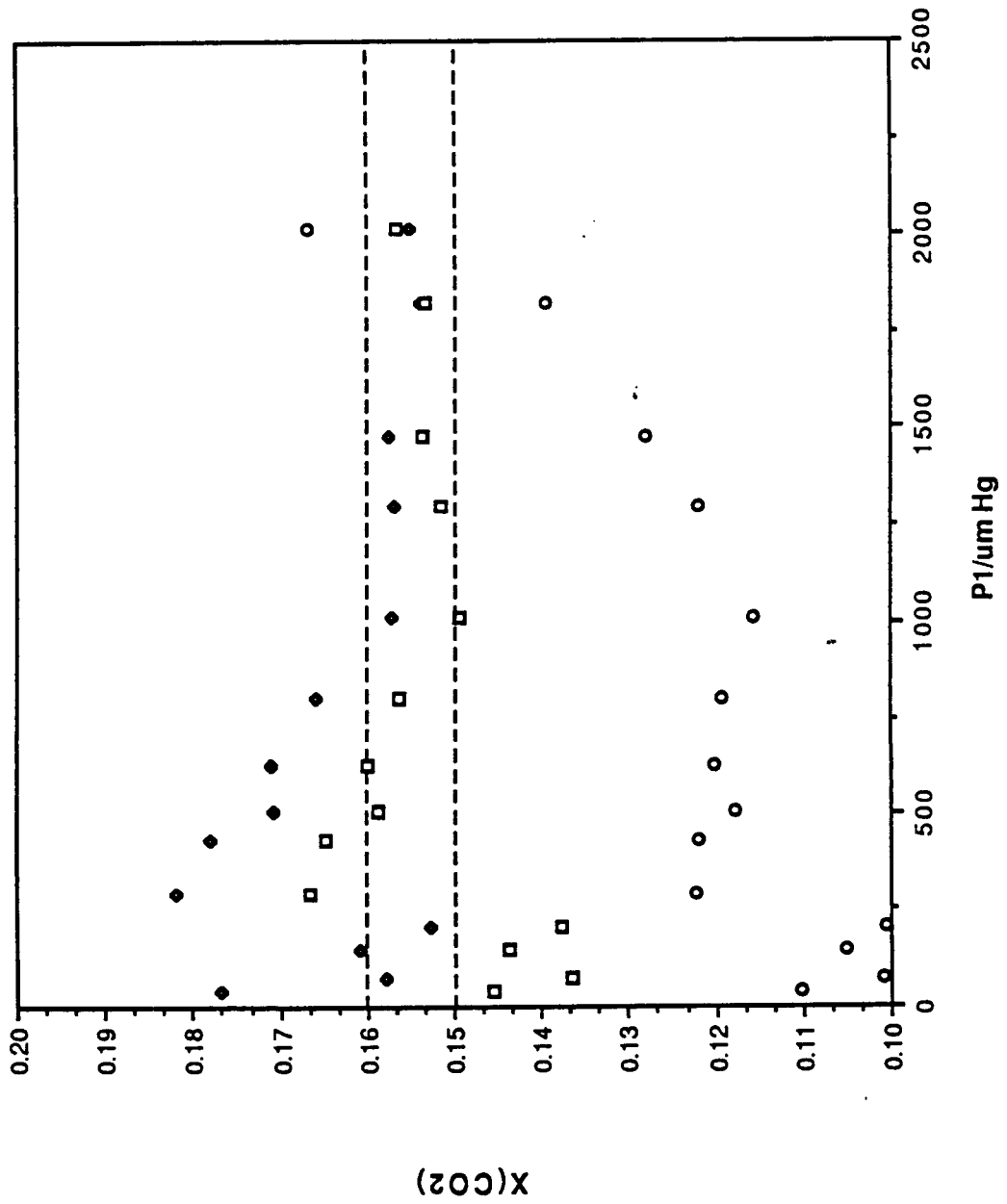
Standards:
3% CO2-air
7% CO2-air
Itself
X(CO2)
0.20
0.19
0.18
0.17
0.16
0.15
0.14
0.13
0.12
0.11
0.10
0
500
1000
1500
2000
2500
P1/um Hg

Figure 27. X_{CO2} from the sample gas containing 3.033% CO_2 in air calculated from data on various standards for the 0.035-mm inlet on the UTI setup.

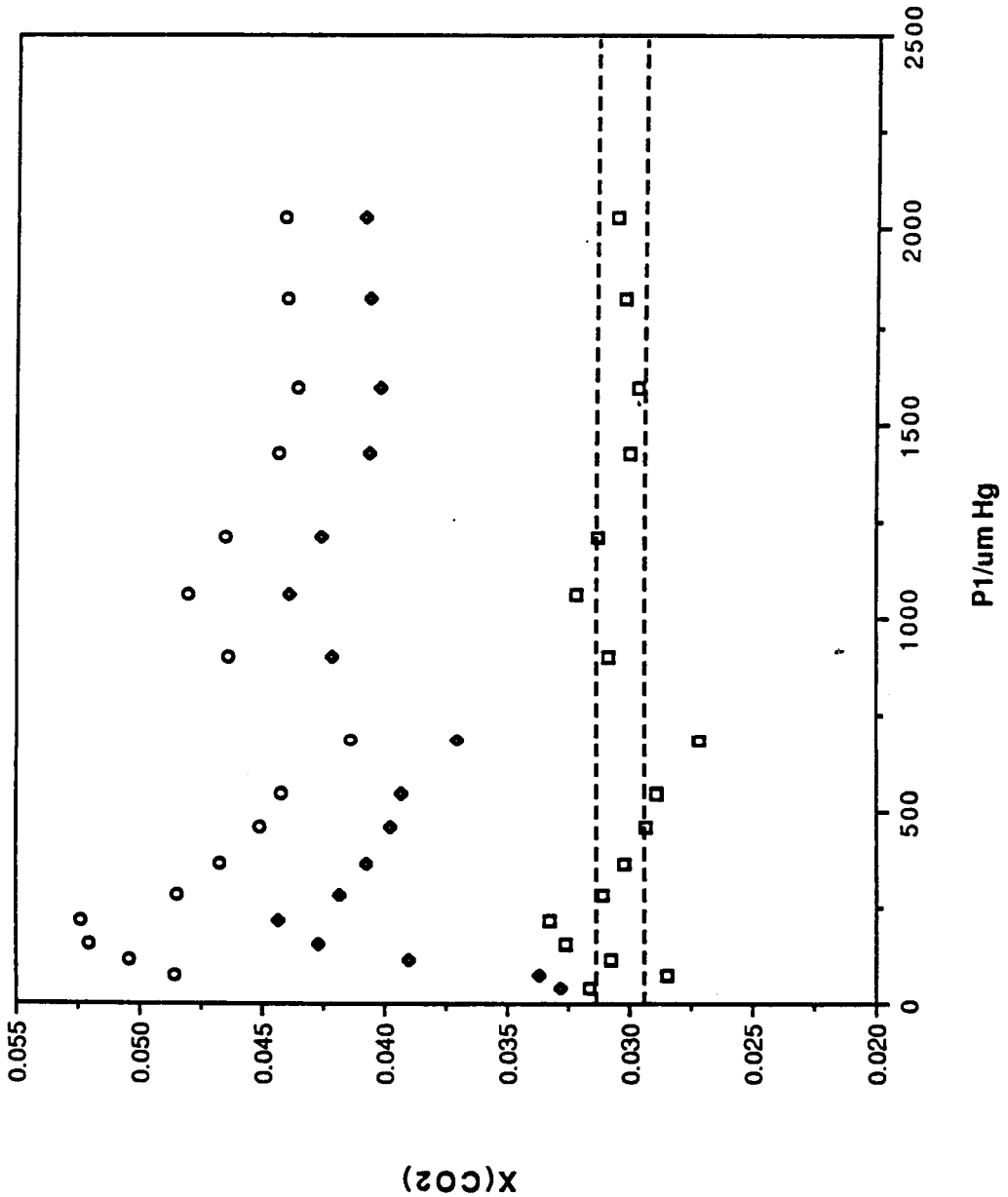
Standards:
7% CO2-air
15% CO2-air
Itself
x(CO2)
0.055
0.050
0.045
0.040
0.035
0.030
0.025
0.020
0
500
1000
1500
2000
2500
P1/um Hg

the random error in the measurement of I_i, then the uncertainty resulting from the calibration curve should be negligible relative to the uncertainty contributed by the measurement of I_i for the sample gas. Considering the sample gas, recall from the Methodology section that ten replicate scans were averaged to give the final I_i. When I_i was measured, if the standard deviation was greater than 3.4%, then the measurement was repeated. In general, the standard deviation was about 1%-2% of the measured I_i, but 3.4% gives an upper limit for the uncertainty in I_i from the sample gas.

For the sample gas containing 9.71% Ne and 9.77% Kr in N_2, the uncertainty in the calculated mole fractions is +/- 0.0033 based on 3.4% of the expected value of each. Therefore, regardless of the standard used we would expect X_{Ne} to range from 0.0938 to 0.1004 and X_{Kr} to range from 0.0944 to 0.1010. The expected range of values for the calculated mole fractions is enclosed by dotted lines as shown on the graphs in Figures 17-27. Inspection of these results shows that the only standard providing values within this range is the sample gas itself. Even here the values obtained at the lowest few pressures are not within the expected +/- 0.0033 uncertainty. Some of the values provided for X_{Ne} and X_{Kr} by the binary and other ternary standard are very close to the expected ranges the majority being within 10% of the

expected values or approximately +/- 0.01. Values provided by the pure gas standards, on the other hand, are not close to the expected values.

These results suggest several conclusions: (1) either the method used to determine the mole fractions is not valid for very low P_1 or that background gases interfere with the measurements at low P_1; (2) the standard must be very near the composition of the sample gas in order to determine the concentrations to within the expected instrumental error; (3) a standard gas can provide reasonably accurate mole fractions, although not within the predicted error, if its composition approximates the sample gas reasonably closely; and (4) the mass discrimination effects are not a product of instrumental error and are a function of the composition of the gas.

DISCUSSION

As evidenced by the theory presented in the introduction, the anomalous enrichment in the heavier species demonstrated by the 9.71% Ne and 9.77% Kr in N_2 cannot be explained on the basis of either diffusive or drift contributions to flow. It is possible, however, that surface diffusion may contribute to our observations as it is likely that Kr, being more polarizable than Ne, would have a greater transport through the sample inlet due to interactions at the face of the MCP and within the capillaries. Using equation 6 for the separation efficiency due to surface adsorption Z_S to calculate the separation efficiency for a mixture of Ne and Kr, we have

$$\Gamma_{Ne}/\Gamma_{Kr} = \exp[(\epsilon_{Ne}-E_{Ne})]/\exp[(\epsilon_{Kr}-E_{Kr})]$$

where the assumption is made that $\sqrt{(F_j/F_i)} = 1$ since Kr and Ne are monatomic. To the best of the author's knowledge, no literature exists on ϵ and E for either Ne or Kr. For a random walk at the surface of the MCP or within a capillary, $\epsilon \approx E$ for both species, otherwise, the species could not become adsorbed ($\epsilon << E$) or would become irreversibly bound to the surface, ($\epsilon >> E$) an

unevidenced possibility as we have observed no residual Kr or Ne upon bakeout of the MS. If we make the further assumptions that ϵ-E for Kr is greater than ϵ-E for Ne and that both values are positive, then $\Gamma_{Ne}/\Gamma_{Kr} < 1$ suggesting an enrichment in Kr over Ne in the lower pressure regimes. Due to the potential proximity in magnitude of ϵ and E, it is unlikely that surface diffusion could completely explain the anomalous enrichment in Kr though it may be partially responsible.

Another potential contribution to the anomalous enrichment in Kr is ion-atom reactions occurring in the ion chamber, such as

$$Kr + Ne^+ \text{ -----> } Kr^+ + Ne \qquad (15a)$$

$$Kr + N_2^+ \text{ -----> } Kr^+ + N_2 \qquad (15b)$$

$$N_2 + Ne^+ \text{ -----> } N_2^+ + Ne \qquad (15c)$$

For the ternary mixtures, it is likely that due to the abundance of N_2, the latter two reactions would contribute to the apparent enrichment in Kr that would not be accounted for using pure gases for calibration of the apparatus. Because the reactions are obviously concentration dependent, using a mixture gas for calibration should account for these reactions as long as the standard gas closely approximates the relative concentrations of the species. Equations developed by McDaniels

(14) which determine the number of ion-atom and/or ion-molecule reactions based on the dimensions and pressure of the ion chamber, the ion mobility, and the ionizing field strength, suggest that no such reactions are occurring in our ion chamber as the pressure is too low (i.e. in the free molecule flow regime). Pressures in the ion chamber are from 10^{-8} to 10^{-5} torr during the course of the experiment. Even at the higher pressures where mass discrimination is unlikely, the pressure is too low for these ion-atom or ion-molecule reactions to occur. Consequently, it is unlikely that the reactions in 15 could be responsible for the enrichment in Kr.

The historical treatment of flow through tubes, capillaries, and orifices has been based on static conditions and to the best of the author's knowledge, no literature exists for flow analysis similar to our treatment. It is understandable then that these treatments would not qualitatively explain the behavior demonstrated in our research. It is probable that flow effects of the source stream need to be considered in explaining the anomalous Kr enrichment. Because ion-atom reactions are not contributing to the enrichment in Kr and because surface diffusion is not completely responsible, we shall discuss the results in terms of the various flow regimes that exist within the apparatus: (1) the ion source, (2) the tubing extending from the inlet holder and into the

ion source, (3) the inlet itself, and (4) the flow in the upstream tubing.

The low pressures existing in the ion source, as mentioned earlier, suggest that the mixture gas is in the molecular flow regime. All treatment of flow in this regime suggest an enrichment in the lighter species, Ne. It is therefore unlikely that the enrichment in Kr is occurring in the ion source.

The tubing extending from the inlet holder is made initially of stainless steel connecting to a quartz tube leading directly into the ion source. The preferential adsorption of Kr to quartz over Ne and N_2 has been discussed earlier and may be partially responsible for the enrichment. In this tubing, the pressure ranges from 0.005 mm to approximately 0.020 mm. The calculated flow for the pure gases based on λ/r ratios (Knudsen number) indicates that Kr is in the slip flow regime whereas Ne and N_2 are initially in the molecular and tending toward the slip flow regime (2). For the sample gases, it is likely that the molecular and slip flow regimes are entered. Again, theory indicates any enrichment favors the lighter species suggesting that the observed enrichment in Kr is <u>not</u> due to flow effects occurring in the tubing connecting the inlet holder to the ion source.

The remaining possibilities for the enrichment in Kr are the inlet itself or the interaction of the inlet with

the flow on the higher pressure side of the inlet, the source stream. Comparison of the results in Figures 10-15 for the straight-through and the flow-by configurations show that the highest ratios are observed when the inlet is in direct contact with the source stream. The only exception is for the MCP-CB which will be discussed later. The straight-through configuration more closely approximates the theoretical treatment discussed in the Theory section as it contains a volume between the source stream and the inlet; this is a quasistatic situation. Although the lower ratios for the straight-through configuration show a greater transport of Ne through the inlet relative to the flow-by configuration, the ratios increase with decreasing pressure. Therefore, even if enrichment in Ne is occurring in the straight-through configuration at the inlet, it does not exceed the enrichment in Kr and cannot explain our observations.

For the flow-by configuration, the inlet can interact directly with the source stream. If we compare the ratios as the size of the mask changes, we can see that the smaller I_{Kr}/I_{Ne} occur for the larger masks, in general. The pumping speed through an orifice is directly proportional to the diameter of the orifice; therefore, the larger the mask, the greater the pumping speed toward the MS. With more pumping speed, a greater volume of sample can be removed from the source stream

and sampling can occur at a greater distance from the surface of the inlet. Consequently, smaller ratios are obtained when sampling occurs at a greater distance from the surface of the inlet. Or in other words, the lighter species, Ne, would appear to be concentrating near the center of the tubing whereas the heavier species, Kr, would appear to be concentrating at the tubing wall. Keep in mind that this would be observed only in the molecular and slip flow regimes where the species in the sample gas can behave approximately independently.

The theoretical basis for the heavier species being concentrated at the tubing wall in the slip flow regime follows that for thermal diffusion where the concentration and velocity (temperature) gradients are parallel rather than perpendicular as in most transport phenomena. The velocity gradient for a gas flowing in a tube is highest at the center where there is the least resistance to flow, and decreases toward the tubing wall. As in thermal diffusion, the lighter species migrates toward the higher velocity region, the center of the tube, and the heavier species migrates toward the lower velocity region, the wall. With Kr concentrated at the wall, we would expect to observe larger ratios for I_{Kr}/I_{Ne} when the orifice is smaller as is observed, except for MCP-CB.

Based on the dimensions of the tube, it seems more

likely that in a given mixture the lighter species, having the longer mean free path, is less likely to collide with the inlet and be swept toward the MS in the lower pressure regimes. The result would be an enrichment in the heavier species. An increase in the size of the mask would increase the probability of collision with the inlet for the lighter species thus increasing its likelihood of being swept toward the MS.

The similarity between ratios for MCP-CB can be explained on the basis of the very small size of the capillaries in this plate. Upon collision with a capillary, its small opening size and increased size at the center would more likely trap an atom than reflect it back into the source stream. As a result, the ratios would be independent of flow considerations suggesting both flow-by and straight-through would have similar ratios. This explains our observations, but there still remains the unexplained enrichment of Kr at lower pressures for this inlet.

CONCLUSION

We have seen that the method presented in this thesis can provide reasonably good estimations of composition for a gas flowing perpendicular to a sample inlet, the flow likely to be encountered by the sample inlet on the tethered satellite. The degree of accuracy increases as the standard gas composition approaches that of the sample gas. Reasonably accurate compositions, like those provided by standards whose composition is reasonably close to the sample gas, should be adequate in adding viscous and real-gas effects to the existing theoretical models used in vehicle design and in calculation of the associated flight parameters. Under these conditions, it is likely that the method of sampling the boundary layer presented in this thesis is viable for various re-entry vehicles at altitudes greater than 90 km.

We have also seen that the majority of the theory on flow through capillaries does <u>not</u> explain the anomalous enrichment in Kr observed during our experimentation. Consequently, further experimentation on inlet effects and surface enrichment or theoretical modeling of the flow outside the sample inlet with respect to the composition of the gas should provide further insight into the

observed mass discrimination effects.

LIST OF REFERENCES

1. Wood, George M., Jr.; Hoppe, John C.; Eide, Donald G.; Lewis, Beverley W. and Brown, Kenneth G.: Candidate Techniques for Non-Intrusive Measurement of Flight Boundary Layer Properties, AIAA 20th Thermophysics Conference, Williamsburg, Virginia, June 19-21, 1985, Paper AIAA-85-0970.

2. Brown, K. G., Fishel, C. E., Brown, D. R., Lewis, B. W., and Wood, G. M.: Development of an Effusive Inlet for Mass Spectometric Gas Analysis of Hypersonic Boundary Layer, ICIASF, '87 Record (1987) 95.

3. Knudsen, M.: The Law of Molecular Flow and Viscosity of Gases Moving Through Tubes, Ann. d. Physik, 28 (1909) 705.

4. Crane, K. C. A. and Stalker, R. J., J. Phys.: Appl. Phys., 10 (1977) 679.

5. Chang, C. and Tiernan, T. O., Final Technical Report, AWFAL-TR-81-2139.

6. Brown, Kenneth G.: Analysis of Flow Dynamics Through Small Diameter Gas Sampling Systems, NASA technical report NAS-1-17099-8, October 1983.

7. Gaede, W.: External Friction of Gases, Ann. d. Physik 41 (1913) 289.

8. Aozumi, H.: Studies in the Flow of Gaseous Mixtures Through Capillaries. II. The Molecular Flow of Gaseous Mixtures, Bull. Chem. Soc., 12 (1937) 285.

9. Pollard, W. G. and Present, R. D.: On gaseous Self-Diffusion in Long Capillary Tubes, Physical Review, 73 (1948) 762.

10. Scott, D. S. and Dullien, F. A. L.: The Flow of Rarefied Gases, A. I. Ch. E Journal, 8 (1962) 293.

11. Pollard, W. G. and DeButhune, A. J.: Separation of a Gaseous Mixture Through a Long Tube at Low Pressure, Physics Review, 75 (1949) 1050.

12. Lund, L. M. and Berman, A. S.: Flow and Self-Diffusion of Gases in Capillaries. I, Journal of Applied Physics, 37 (1966) 2489.

LIST OF REFERENCES (cont.)

13. Ishida, K., Shimokawa, J. and Yamamoto, Y.: Effect of the Surface Diffusion on the Separation Efficiency, Faraday Society Transactions, 5 (1961) 2018.

14. McDaniel, E. W.; The Mobility and Diffusion of Ions in Gases, Ch. 1, John Wiley and Sons, New York, 1973.

APPENDIX A

This appendix contains the C-50 computer program used to collect and store the data as well as to calculate pertinent quantities used in assessing the data.

```
10 CLS
20 PRINT "          This is program IBMADC10: computerized data aquisition"
30 PRINT "     of mass spectra from the EXTRANUCLEAR C50.  Because a mass"
40 PRINT "     calibration is absent, the sampling rate must be set at ten"
50 PRINT "     points per second.  Also for best results, a scan rate of "
60 PRINT "     either 1 or 0.5 amu per seconds should be used."
70 PRINT "          If the error message ''Error in setting AIN rate'' occurs"
80 PRINT "     during a scan, hit (ctrl-break), (return) and restart the pro-"
90 PRINT "     gram."\ PRINT
100 DIM INBUF (2000,12),FPK%(20),P(2000),N$(20),DV(50),IV(50),D$(10)
110 DIM PEAK(50),MV(50),RUN(50),P1(50),P2(50),PMS(50),FL(50),PK(50)
120 DIM PK1(50),PK2(50),PK3(50),PK4(50),PK5(50),BG(2000),SRT(50)
130 DIM V(40),SD(40),PR1(40),PR2(40),PR3(40),ZE(40),S1(50),S2(50),S3(50)
140 DIM SD1(40),SD2(40),SD3(40),SD4(40),SD5(40)
150 INPUT "      ENTER THE FILE NAME FOR THIS SET OF DATA: ";Q$
160 R=0\ OPEN Q$ AS FILE #6    ! R IS THE RUN COUNTER
170 ON ERROR GOTO 240
180 FOR U=1 TO 50
190 INPUT #6, FL(U),P1(U),P2(U)
200 INPUT #6, PMS(U),PK1(U),PK2(U)
210 INPUT #6, PK3(U),PK4(U),PK5(U)
220 R=R+1
230 NEXT U
240 IF ERR=11 THEN RESUME 250
250 CLOSE #6
260 ON ERROR GOTO 420
270 INPUT "PRESS RETURN TO CONTINUE OR E TO EXIT  ";C$
280 IF C$="E" GOTO 4440
290 CLS\PRINT"(1) SCAN SPECTRUM WITH NEW PARAMETERS"
300 PRINT "(2) SCAN SPECTRUM WITH SAME PARAMETERS"
310 PRINT "(3) CHANGE MASS RANGE"
320 PRINT "(4) DISPLAY DATA"
330 PRINT "(5) LIST TABLE OF CURRENT RESULTS"
340 PRINT "(6) CHOOSE MAJOR PEAKS AGAIN"
350 PRINT "(7) PLOT CURRENT RESULTS AT CRT"
360 PRINT "(8) FILE RESULTS"
370 PRINT "(9) SENSITIVITY CALCULATIONS AND HARD COPY OF RESULTS"
380 PRINT "(10) HARD COPY OF RESULTS"
390 PRINT "(11) SET ZERO-POINT FOR IONIZATION GAUGE SCALES"
400 PRINT "(12) EXIT"
410 INPUT "CHOOSE A FUNCTION BY PRESSING THE NUMBER  ";NUMB
420 IF ERR=58 THEN RESUME 260
430 ON NUMB GOTO 440,580,550,1930,1990,1400,2200,3250,3340,3870,4330,4440
440 CLS \ PRINT "****************PROGRAM IBMADC10*****************"
450 INPUT "ENTER DATE ";DT$
460 INPUT "ENTER SAMPLE BEING RUN ";GAS$
470 INPUT "ENTER CONDITIONS: ";CD$
480 INPUT "ENTER NUMBER OF PEAKS TO BE MONITORED, UP TO 5 ";NP
490 FOR J=1 TO NP
500  INPUT "ENTER PEAK AMU: ";AMU(J)
510 NEXT J
520 INPUT "INPUT SCAN RATE (AMU/SEC) ";SCR
```

```
530 INPUT "INPUT SAMPLING RATE (PTS/SEC) ";SMR
540 INPUT "INPUT NO. OF SCANS ";SN
550 INPUT "INPUT LOWER MASS ";LM
560 INPUT "INPUT UPPER MASS ";UM
570 PT=(UM-LM)/SCR*SMR \ PT=INT(PT)
580 PRINT\PRINT PT;"DATA PTS WILL BE COLLECTED FOR EACH SCAN"
590 FOR X=1 TO PT
600  INBUF(X,0)=0
610 NEXT X
620 FOR Y=1 TO SN
630 OPEN "$ADC00" AS FILE #12
640 FPK%(1)=4
650 FPK%(2)=0
660 FPK%(3)=-1
670 FPK%(4)=1
680 FPK%(5)=1
690 FPK%(6)=0
700 FPK%(7)=2
710 FPK%(8)=0
720 FPK%(9)=3
730 FPK%(10)=0
740 CALL SYSFUNC(12,FPK%(1))   !SETS A/D PARAMETERS
750 LED2 = -1
760 CALL SYSOPEN (100,"$LED00",0.0,0,0,LED2)
770 CALL BWRITE (LED2,1)  ! SENDS +5V TO C50 RESET
780 WAIT(2)
790 CALL BWRITE (LED2,0)  !TERMINATES +5V TO C50 RESET
800 CALL SYSCLOSE (100)
810 PRINT Y;" ";
820 FOR X=1 TO PT
830 CALL AIN (12,SMR,1,1,INBUF(X,Y))   !START A/D CONVERTER
840 NEXT X
850 FOR X=1 TO PT
860 INBUF(X,0)=INBUF(X,0)+INBUF(X,Y)
870 NEXT X
880 CLOSE #12
890 NEXT Y
900 PRINT " "
910 FOR X=1 TO PT
920 P(X)= LM + X*(SCR/SMR)
930 INBUF(X,0)=INBUF(X,0)/SN        ! AVERAGES DATA
940 NEXT X
950 PR3(0)=0
960 OPEN "$ADC01" AS FILE #11
970 CALL AIN(11,30,1,30,PR3(1))
980 FOR J=1 TO 30
990  PR3(0)=PR3(0)+PR3(J)
1000 NEXT J
1010  PR3(0)=PR3(0)/30000 - PR3(0)
1020 CLOSE #11
1030 OPEN "$KPD" AS FILE #8
```

```
1040 CALL SYSFUNC(8,FPK%(7))   !TURNS ON BEEPER
1050 WAIT (10)
1060 CALL SYSFUNC(8,FPK%(9))   !TURNS OFF BEEPER
1070 CLOSE #8
1080 REM ***REMOVES VOLTAGE SPIKES***
1090 V=PT
1100 FOR X=1 TO PT
1110 IF INBUF(X,0)<1048576 AND INBUF(X,0)>-100 GOTO 1190
1120   FOR W=X TO V-1
1130   INBUF(W,0)=INBUF(W+1,0)
1140   P(W)=P(W+1)
1150   NEXT W
1160 IF W>=PT GOTO 1200
1170 X=X-1
1180 V=V-1
1190 NEXT X
1200 PRINT "THERE WERE ";PT-V;" SPIKES REMOVED.  ";
1210 PRINT V;" POINTS REMAIN."\PRINT
1220 REM ***LOCATES MAJOR PEAKS***
1230 PC=0
1240 FOR S=1 TO 40
1250  V(S)=0
1260 NEXT S
1270 FOR X=1 TO PT-2
1280   IF INBUF(X,0)<2000 GOTO 1390
1290   DIF1=INBUF(X+1,0)-INBUF(X,0)
1300   DIF2=INBUF(X+2,0)-INBUF(X+1,0)
1310   IF DIF1>=0 AND DIF2<0 THEN 1320 ELSE 1390
1320   PC=PC+1
1330 FOR Y=1 TO SN
1340  V(PC)=V(PC)+(INBUF(X+1,Y)-INBUF(X+1,0))**2  !SUM OF SQUARES OF VARIENCES
1350 NEXT Y
1360   SD(PC)=SQR(V(PC)/(SN-1))  !STANDARD DEVIATION
1370   PEAK(PC)=P(X+1)
1380   MV(PC)=INBUF(X+1,0)
1390 NEXT X
1400 PRINT"MAJOR PEAKS OCCUR AT..."
1410 PRINT"MASS(AMU)       INTENSITY(MICROVOLTS)"
1420 FOR T=1 TO PC
1430   PRINT "(";T;") ";PEAK(T),MV(T);"+/-";SD(T),SD(T)/MV(T)*100
1440 NEXT T
1450 INPUT "SAVE PEAKS? <Y> ";SP$
1460 IF SP$="N" THEN 1610
1470 INPUT "ENTER AMU ASSIGNMENT (1-5)";AA
1480 INPUT "ENTER PEAK NUMBER ";PKN
1490 TMP=MV(PKN)/1048.576  \ TI=SD(PKN)/1048.576
1500 ON AA GOTO 1510,1530,1550,1570,1590
1510 PK1(R+1)=TMP \ SD1(R+1)=TI
1520 GOTO 1450
1530 PK2(R+1)=TMP \ SD2(R+1)=TI
```

```
1540 GOTO 1450
1550 PK3(R+1)=TMP \ SD3(R+1)=TI
1560 GOTO 1450
1570 PK4(R+1)=TMP \ SD4(R+1)=TI
1580 GOTO 1450
1590 PK5(R+1)=TMP \ SD5(R+1)=TI
1600 GOTO 1450
1610 INPUT "SCAN AGAIN? <N> ";SC$
1620 IF SC$="Y" THEN 550
1630 PRINT\ IF NUMB=6 THEN R=R ELSE R=R+1
1640 INPUT "SET CHANNEL TO READ P1 THEN HIT <RETURN>. ";RT$
1650 OPEN "#ADC02" AS FILE #10
1660 PR2(0)=0 \ PR1(0)=0
1670 CALL AIN(10,30,1,30,PR1(1))
1680 FOR J=1 TO 30
1690  PR1(0)=PR1(0)+PR1(J)
1700 NEXT J
1710  P1(R)=PR1(0)/3000/1.048576
1720 INPUT "SET CHANNEL TO READ P2 THEN HIT <RETURN>. ";RT$
1730 CALL AIN(10,30,1,30,PR2(1))
1740 FOR J=1 TO 30
1750  PR2(0)=PR2(0)+PR2(J)
1760 NEXT J
1770  P2(R)=PR2(0)/3000/1.048576
1780 CLOSE #10
1790 INPUT "IS SCALE 10^-8 <1>, 10^-7 <2>, 10^-6 <3>, OR 10^-5 <4>? ";SCALE
1800 ON SCALE GOTO 1810,1830,1850,1870
1810  PMS(R)=PR3(0)/100
1820   GOTO 1880
1830  PMS(R)=PR3(0)/10
1840   GOTO 1880
1850  PMS(R)=PR3(0)
1860 GOTO 1880
1870 PMS(R)=PR3(0)*10
1880 IF GAS$="NE" THEN PMS(R)=PMS(R)*4.22   !CORRECTS FOR PURE NE
1890 IF GAS$="KR" THEN PMS(R)=PMS(R)*.53    !CORRECTS FOR PURE KR
1900 IF GAS$="CO2" THEN PMS(R)=PMS(R)*0.73
1903 IF GAS$="10.1% NE, 8.06% KR IN N2" THEN PMS(R)=PMS(R)*1.29
1904 IF GAS$="5.08% NE, 14.9%KR IN N2" THEN PMS(R)=PMS(R)*1.09
1905 IF GAS$="HE" THEN PMS(R)=PMS(R)*6.22
1907 IF GAS$="52.5% NE IN KR" THEN PMS(R)=PMS(R)*2.47
1908 IF GAS$="9.93% NE IN N2" THEN PMS(R)=PMS(R)*1.32
1909 IF GAS$="9.85% KR IN N2" THEN PMS(R)=PMS(R)*0.954
1910 INPUT "ENTER FLOW IN SCCM ";FL(R)
1920 GOTO 260
1930 REM ***DISPLAYS DATA***
1940 CLS\PRINT "MASS (AMU)       INTENSITY (MICROVOLTS)"
1950 FOR X=1 TO PT
1960 PRINT P(X),INBUF(X,G       : PRINTS DATA ON CRT
1970 NEXT X
1980 GOTO 260
```

```
1990 REM ***PRINTS RESULTS OF LATEST RUNS AT CRT***
2000 CLS\PRINT " RESULTS OF THE LATEST RUNS SCALED TO MILLIVOLTS"\ PRINT
2010 PRINT " FLOW     P1      P2      PMS       1        2        3  ";
2020 PRINT "      4       5    "
2030 PRINT " SCCM      u       u     1000u     mV       mV       mV";
2040 PRINT "       mV       mV"
2050 FOR Q=1 TO R
2060 PRINT USING "##.##  ####.#  ####.#   ##.###";FL(Q),P1(Q),P2(Q),PMS(Q);
2070 PRINT USING "  ####.##  ####.##  ####.##";PK1(Q),PK2(Q),PK3(Q);
2080 PRINT USING "  ####.##   ####.##";PK4(Q),PK5(Q)
2090 NEXT Q
2100 PRINT \ PRINT
2110 PRINT " P1/u      184/120      184/114      120/114      142/184"
2120 FOR J= 1 TO R
2130  PRINT USING "####.##      ##.####      ";P1(J),PK4(J)/PK2(J);
2140  PRINT USING "##.####      ##.####";PK4(J)/PK1(J), PK2(J)/PK1(J);
2150  PRINT USING "      ##.####" PK3(J)/PK4(J)
2160 NEXT J
2170 INPUT "DELETE LAST POINT? <N>";C$
2180 IF C$="Y" THEN R=R-1
2190 GOTO 260
2200 REM ***GRAPHS DATA ON CRT***
2210 CLS \ INPUT "ENTER PEAK ASSIGNMENT NUMBER: ";ASS
2220 ON ASS GOTO 2230,2270,2310,2350,2390
2230 FOR P=2 TO R
2240  DV(P)=PK1(P)\ SRT(P)=DV(P)
2250 NEXT P
2260 GOTO 2420
2270 FOR P=2 TO R
2280  DV(P)=PK2(P) \ SRT(P)=DV(P)
2290 NEXT P
2300 GOTO 2420
2310 FOR P=2 TO R
2320  DV(P)=PK3(P) \ SRT(P)=DV(P)
2330 NEXT P
2340 GOTO 2420
2350 FOR P=2 TO R
2360  DV(P)=PK4(P)\ SRT(P)=DV(P)
2370 NEXT P
2380 GOTO 2420
2390 FOR P=2 TO R
2400  DV(P)=PK5(P)\ SRT(P)=DV(P)
2410 NEXT P
2420 INPUT "IS A SENSITIVITY DESIRED? <Y/N> ";SD$
2430 IF SD$="N" THEN 2570
2440 INPUT "ENTER PRESSURE DESIRED: P1, P2, PMS <1,2,3> ";SS
2450 ON SS GOTO 2460,2500,2540
2460 FOR P=2 TO R
2470  DV(P)=DV(P)/P1(P) \ SRT(P)=DV(P)
```

```
2480 NEXT P
2490 GOTO 2570
2500 FOR P=2 TO R
2510  DV(P)=DV(P)/P2(P) \ SRT(P)=DV(P)
2520 NEXT P
2530 GOTO 2570
2540 FOR P=2 TO R
2550  DV(P)=DV(P)/PMS(P) \ SRT(P)=DV(P)
2560 NEXT P
2570 PRINT\ PRINT "(1) P1"\ PRINT "(2) P2"\ PRINT "(3) Pms"
2580 INPUT "ENTER NUMBER OF INDEPENDENT VARIABLE ";B
2590 ON B GOTO 2600,2640,2680
2600 FOR P=2 TO R
2610  IV(P)=P1(P)
2620 NEXT P
2630 GOTO 2710
2640 FOR P=2 TO R
2650  IV(P)=P2(P)
2660 NEXT P
2670 GOTO 2710
2680 FOR P=2 TO R
2690  IV(P)=PMS(P)
2700 NEXT P
2710 INPUT "LOG(10) SCALE FOR X-AXIS? <N>";LS$
2720 IF LS$="Y" THEN 2730 ELSE 2760
2730 FOR P=1 TO R
2740   IV(P)=LOG(IV(P))
2750 NEXT P
2760 REM  SORTING OF DV TO FIND MAX AND MIN VALUES
2770 FOR P=2 TO R-1
2780  IF SRT(P)<=SRT(P+1) THEN 2800
2790 MAX=SRT(P)\ SRT(P)=SRT(P+1)\ SRT(P+1)=MAX
2800 MAX=SRT(P+1)
2810 NEXT P
2820 MAX=-1*INT(-1*MAX)
2830 FOR P=2 TO R-1
2840  IF SRT(P)>=SRT(P+1) THEN 2860
2850 MIN=SRT(P)\ SRT(P)=SRT(P+1)\ SRT(P+1)=MIN
2860 NEXT P
2870 MIN=INT(MIN)
2880 REM CRT GRAPHICS
2890 PX=685/(IV(R)-IV(2))
2900 XTIC=20\ XT=34.25\ MXT=68.5
2910 PY=420/(MAX-MIN)
2920 YTIC=20\ YT=21\ MYT=42
2930 CLS
2940 OPEN "#GR" AS FILE #7
2950 REM AXES
2960 LINE(57,47,742,47)
2970 LINE(57,47,57,467)
```

```
2980 FOR J=57 TO 742 STEP 34.25
2990 LINE(J,42,J,51)
3000 NEXT J
3010 F=IV(2)
3020 FOR J=57 TO 742 STEP 68.5
3030 LINE(J,37,J,56)
3040 G=F
3050 TEXT((J-3),14,NUMI$(G))
3060 F=F+((IV(R)-IV(2))/10)\ F=INT(1000*F)/1000
3070 NEXT J
3080 FOR J=47 TO 467 STEP 21
3090 LINE(52,J,61,J)
3100 NEXT J
3110 D=MIN\ D=INT(1000*D)/1000
3120 FOR J=47 TO 467 STEP 42
3130 LINE(47,J,66,J)
3140 TEXT(24,(J-3),NUMI$(D))
3150 D=D+((MAX-MIN)/10)
3160 NEXT J
3170 FOR J=1 TO R
3180 X1=(IV(J)*PX)+57-(IV(2)*PX)
3190 Y1=(DV(J)*PY)-MIN*PY+47
3200 LINE (X1,Y1,X1,Y1)
3210 ELLIPSE (X1,Y1,X1+2,Y1+2)
3220 NEXT J
3230 CLOSE #7
3240 GOTO 260
3250 REM ***FILES RESULTS OF LATEST RUN***
3260 OPEN Q$ AS FILE #4
3270 FOR T=1 TO R
3280 PRINT #4, FL(T),",",P1(T),",",P2(T)
3290 PRINT #4 PMS(T),",",PK1(T),",",PK2(T)
3300 PRINT #4 PK3(T),",",PK4(T),",",PK5(T)
3310 NEXT T
3320 CLOSE #4
3330 GOTO 410
3340 REM ***CALCULATES SENSITIVITIES AND PRINTS PESULTS TO PRINTER***
3350 INPUT "WHICH AMU ASSIGNMENT: 1,2,3,4,5 ";WS
3360 INPUT "ENTER MOLE FRACTION OF SPECIES TO CORRECT PRESSURE: ";MF
3370 ON WS GOTO 3380,3450,3520,3590,3660
3380  FOR J=1 TO R
3390   PK(J)=PK1(J)
3400   S1(J)=PK1(J)/P1(J)/MF
3410   S2(J)=PK1(J)/P2(J)/MF
3420   S3(J)=PK1(J)/PMS(J)/MF
3430  NEXT J
3440  GOTO 3720
3450  FOR J=1 TO R
3460   PK(J)=PK2(J)
3470   S1(J)=PK2(J)/P1(J)/MF
3480   S2(J)=PK2(J)/P2(J)/MF
3490   S3(J)=PK2(J)/PMS(J)/MF
```

```
3500  NEXT J
3510  GOTO 3720
3520  FOR J=1 TO R
3530   PK(J)=PK3(J)
3540   S1(J)=PK3(J)/P1(J)/MF
3550   S2(J)=PK3(J)/P2(J)/MF
3560   S3(J)=PK3(J)/PMS(J)/MF
3570  NEXT J
3580  GOTO 3720
3590  FOR J=1 TO R
3600   PK(J)=PK4(J)
3610   S1(J)=PK4(J)/P1(J)/MF
3620   S2(J)=PK4(J)/P2(J)/MF
3630   S3(J)=PK4(J)/PMS(J)/MF
3640  NEXT J
3650  GOTO 3720
3660  FOR J=1 TO R
3670   PK(J)=PK5(J)
3680   S1(J)=PK5(J)/P1(J)/MF
3690   S2(J)=PK5(J)/P2(J)/MF
3700   S3(J)=PK5(J)/PMS(J)/MF
3710  NEXT J
3720 INPUT "ENTER TITLE OF TABLE: ";TTL$
3730 PRINT #5 TTL$
3740 PRINT #5
3750 PRINT #5 "  I       P1     S(P1)    P2       S(P2)     PMS  10^-3 S(PMS)"
3760 PRINT #5 "  mV      um     mV/um    um       mV/um      um      mV/u"
3770 PRINT #5
3780 FOR B=1 TO R
3790 PRINT #5 USING "###.##  ####.#  ##.###   ##.#";PK(B),P1(B),S1(B),P2(B);
3800 PRINT #5 USING "    ###.##    ##.###   ###.#";S2(B),PMS(B),S3(B)
3810 NEXT B
3820 INPUT "ANOTHER COPY? ";AC$
3830 IF AC$="Y" THEN 3720
3840 INPUT "CALCULATE SENSITIVITIES FOR ANOTHER SPECIES? ";AS$
3850 IF AS$="Y" THEN GOTO 3340
3860 GOTO 410
3870 REM***HARD COPY OF RESULTS***
3880 OPEN "$SER00" AS FILE #5
3890 INPUT "DO YOU WANT A COPY OF 99% CONFID. LEVELS? ";CL$
3900 IF CL$="N" THEN 4000
3910 PRINT #5 "I";AMU(1)," ","I";AMU(2)," ","I";AMU(3)
3920 FOR J=1 TO R
3930 PRINT #5 PK1(J);"+/-";SD1(J),PK2(J);"+/-";SD2(J),PK3(J);"+/-";SD3(J)
3940 NEXT J
3950 PRINT #5 \ PRINT #5 \ PRINT #5
3960 PRINT #5 "I";AMU(4)," ","I";AMU(5)
3970 FOR J=1 TO R
3980 PRINT #5 PK4(J);"+/-";SD4(J),PK5(J);"+/-";SD5(J)
```

```
3990 NEXT J
4000 INPUT "DO YOU WANT A HARD COPY OF THE RAW DATA? ";HC$
4010 IF HC$="N" THEN 4210
4020 PRINT #5 "DATE: ";DT$;"   SAMPLE: ";GAS$
4030 PRINT #5 "CONDITIONS: ";CD$
4040 PRINT #5 "FILE: ";Q$
4050 PRINT #5 "MICROCHANNEL PLATE CODE: NONE"\PRINT #5 "MASK CODE 50u"
4060 PRINT #5 "EMMISION CURRENT: 1.80 mA"
4070 PRINT #5 "IONIZATION POTENTIAL: 70.0 eV"
4080 PRINT #5 "MULTIPLIER SENSITIVITY: -1.00 kV"
4090 PRINT #5 "NUMBER OF SCANS AVERAGED ";SN
4100 PRINT #5
4110 PRINT #5 " FLOW     P1      P2      PMS     I";AMU(1);"    I";AMU(2);
4120 PRINT #5 "    I";AMU(3);"    I";AMU(4);"     I";AMU(5)
4130 PRINT #5 " SCCM     um      um     1000um    mV       mV       mV " ;
4140 PRINT #5 "       mV       mV"
4150 PRINT #5
4160 FOR B=1 TO R
4170 PRINT #5 USING "##.##  ####.#  ####.#   ##.###";FL(B),P1(B),P2(B),PMS(B);
4180 PRINT #5 USING "  ####.##  ####.##  ####.##";PK1(B),PK2(B),PK3(B);
4190 PRINT #5 USING "  ####.##   ####.##";PK4(B),PK5(B)
4200 NEXT B
4210 PRINT #5 \ PRINT #5 \ PRINT #5
4220 INPUT "HARD COPY OF RATIOS? ";HR$
4230 IF HR$="N" THEN 4300
4240 PRINT #5 "  P1/um      I84/I20      I84/I14      I20/I14      I42/I84"
4250 FOR J= 1 TO R
4260  PRINT #5 USING "####.##      ##.####      ";P1(J),PK4(J)/PK2(J);
4270  PRINT #5 USING "##.####      ##.####";PK4(J)/PK1(J), PK2(J)/PK1(J);
4280  PRINT #5 USING "      ##.####" PK3(J)/PK4(J)
4290 NEXT J
4300 INPUT "ANOTHER COPY? ";AC$
4310 IF AC$="Y" THEN 3890
4320 GOTO 410
4330 REM ***SETS ZERO-POINT FOR ION. PRES. GUAGE SCALES***
4340 OPEN "#ADC01" AS FILE #9
4350 INPUT "ZERO ON SHORT THEN HIT <RETURN>. ";RT$
4360 CALL AIN(9,30,1,30,ZE(1))
4370 FOR J=1 TO 30
4380  ZE(0)=ZE(0)+ZE(J)
4390 NEXT J
4400 ZE(0)=ZE(0)/30000
4410 PRINT "ZPC= ";ZE(0);" um"
4420 CLOSE #9
4430 GOTO 410
4440 INPUT "ARE YOU SURE YOU STORED YOUR DATA? <Y\N> ";SD$
4450 IF SD$="N" THEN 3250
4460 CLS\END
```

APPENDIX B

This appendix contains the summary tables of the calculated mole fractions for the 5.08% Ne and 14.9% Kr in N_2 and the 3.033% CO_2-, 7.55% CO_2-, and 15.44% CO_2-air mixtures. This data has been presented graphically during the course of the text in Figures 21-27.

TABLE B1. Summary of calculated X(i) for sample gas containing 5.08% Ne and 14.9% Kr in N2 using various standards for the 0.050-mm mask inlet

Total P1	Pure Ne and Kr		Ne-N2 and Kr-N2		10% Ne, 10% Kr in N2		5% Ne, 15% Kr in N2	
μm Hg	X(Ne)	X(Kr)	X(Ne)	X(Kr)	X(Ne)	X(Kr)	X(Ne)	X(Kr)
17.9	-0.0988	0.0537	0.0417	0.1513	0.0389	0.1722	0.0524	0.1513
32.7	-0.0332	0.0877	0.0492	0.1632	0.0443	0.1718	0.0525	0.1670
53.1	-0.0038	0.0968	0.0514	0.1600	0.0457	0.1638	0.0515	0.1655
78.1	0.0086	0.0946	0.0493	0.1491	0.0435	0.1512	0.0482	0.1552
118.4	0.0211	0.0944	0.0523	0.1437	0.0459	0.1454	0.0500	0.1508
161.6	0.0274	0.0946	0.0539	0.1420	0.0471	0.1446	0.0511	0.1501
225.4	0.0317	0.0953	0.0546	0.1424	0.0476	0.1478	0.0518	0.1522
291.2	0.0326	0.0926	0.0532	0.1388	0.0463	0.1478	0.0507	0.1500
383.9	0.0336	0.0864	0.0527	0.1306	0.0457	0.1451	0.0508	0.1434
444.8	0.0334	0.0859	0.0519	0.1312	0.0448	0.1536	0.0504	0.1463
543.7	0.0336	0.0849	0.0516	0.1326	0.0444	0.1536	0.0510	0.1527

TABLE B2. Summary of calculated X(i) for sample gas containing 5.08% Ne and 14.9% Kr in N2 using various standards for the 0.050-mm masked MCP-CB inlet

Total P1	Pure Ne and Kr		Ne-N2 and Kr-N2		10% Ne, 10% Kr in N2		5% Ne, 15% Kr in N2	
μm Hg	X(Ne)	X(Kr)	X(Ne)	X(Kr)	X(Ne)	X(Kr)	X(Ne)	X(Kr)
17.0	-0.0342	-0.0713	0.0248	0.2276	0.0271	0.1948	0.0266	0.1134
29.8	-0.1609	0.0268	0.0432	0.1903	0.0480	0.1658	0.0438	0.1194
44.5	-0.0859	0.1297	0.0482	0.2287	0.0537	0.2027	0.0484	0.1715
65.8	-0.0366	0.1542	0.0512	0.2145	0.0572	0.1915	0.0512	0.1703
89.7	-0.0107	0.1549	0.0516	0.1949	0.0578	0.1747	0.0515	0.1590
118.6	0.0087	0.1640	0.0537	0.1893	0.0602	0.1706	0.0535	0.1586
172.8	0.0260	0.1687	0.0543	0.1799	0.0610	0.1632	0.0541	0.1547
240.8	0.0340	0.1710	0.0524	0.1731	0.0590	0.1582	0.0523	0.1518
341.8	0.0425	0.1723	0.0532	0.1671	0.0601	0.1541	0.0532	0.1492
439.2	0.0441	0.1761	0.0512	0.1661	0.0580	0.1546	0.0513	0.1504
556.0	0.0467	0.1753	0.0509	0.1617	0.0579	0.1520	0.0513	0.1482
654.0	0.0473	0.1779	0.0501	0.1615	0.0572	0.1532	0.0506	0.1495
847.0	0.0485	0.1777	0.0494	0.1574	0.0567	0.1519	0.0502	0.1483
959.2	0.0493	0.1775	0.0494	0.1553	0.0570	0.1513	0.0505	0.1476
1127.3	0.0490	0.1793	0.0484	0.1540	0.0562	0.1525	0.0498	0.1485
1283.9	0.0501	0.1803	0.0490	0.1524	0.0571	0.1532	0.0507	0.1488
1454.7	0.0508	0.1821	0.0493	0.1513	0.0579	0.1547	0.0515	0.1499

TABLE B3. Summary of calculated X(i) for sample gas containing 7.55% CO2 in air using various CO2 in air standards for the 0.035-mm mask inlet

Total P1	3.033% CO2 in air		15.44% CO2 in air		7.55% CO2 in air	
μm Hg	X(CO2)	X(O2)	X(CO2)	X(O2)	X(CO2)	X(O2)
43.5	0.0507	0.3615	0.0629	0.2703	0.0852	0.2901
72.2	0.0505	0.2489	0.0658	0.1939	0.0817	0.2163
109.5	0.0473	0.1984	0.0629	0.1620	0.0751	0.1880
179.5	0.0468	0.1560	0.0633	0.1335	0.0729	0.1604
248.6	0.0504	0.1594	0.0688	0.1423	0.0776	0.1756
314.4	0.0465	0.1591	0.0635	0.1447	0.0712	0.1800
511.2	0.0446	0.1588	0.0611	0.1473	0.0675	0.1835
685.8	0.0541	0.1653	0.0737	0.1537	0.0804	0.1897
875.7	0.0521	0.1638	0.0707	0.1518	0.0767	0.1854
1200.2	0.0522	0.1907	0.0701	0.1736	0.0754	0.2058
1607.4	0.0534	0.1892	0.0706	0.1691	0.0752	0.1962
2035.7	0.0554	0.1933	0.0717	0.1691	0.0755	0.19201

TABLE B4. Summary of calculated X(i) for sample gas containing 15.44% CO_2 in air using various CO_2 in air standards for the 0.035-mm mask inlet

Total P1	3.033% CO_2 in air		7.55% CO_2 in air		15.44% CO_2 in air	
μm Hg	X(CO_2)	X(O_2)	X(CO_2)	X(O_2)	X(CO_2)	X(O_2)
39.4	0.1103	0.3932	0.1767	0.3125	0.1455	0.2926
75.4	0.1010	0.2508	0.1578	0.2236	0.1363	0.1980
146.6	0.1051	0.1847	0.1608	0.1881	0.1437	0.1571
207.8	0.1007	0.1923	0.1526	0.2121	0.1378	0.1719
294.1	0.1223	0.1810	0.1820	0.2059	0.1667	0.1653
430.6	0.1219	0.1700	0.1781	0.1963	0.1648	0.1574
502.1	0.1178	0.1767	0.1709	0.2042	0.1586	0.1642
624.2	0.1201	0.1754	0.1711	0.2061	0.1600	0.1632
804.8	0.1192	0.1842	0.1659	0.2079	0.1564	0.1706
1010.9	0.1158	0.2023	0.1571	0.2214	0.1494	0.1852
1294.9	0.1220	0.2053	0.1569	0.2172	0.1515	0.1852
1477.0	0.1281	0.2059	0.1575	0.2135	0.1537	0.1840
1824.3	0.1396	0.1995	0.1539	0.2009	0.1532	0.1757
2015.4	0.1670	0.2006	0.1552	0.1983	0.1567	0.1750

TABLE B5. Summary of calculated X(i) for sample gas containing 3.033% CO_2 in air using various CO_2 in air standards for the 0.035-mm mask inlet

Total P1	7.55% CO_2 in air		15.44% CO_2 in air		3.033% CO_2 in air	
μm Hg	X(CO_2)	X(O_2)	X(CO_2)	X(O_2)	X(CO_2)	X(O_2)
41.2	0.0579	0.3284	0.0328	0.3152	0.0316	0.3741
76.2	0.0486	0.2384	0.0337	0.2158	0.0285	0.2489
114.6	0.0504	0.2115	0.0390	0.1833	0.0308	0.2065
156.7	0.0521	0.2360	0.0427	0.1959	0.0326	0.2149
215.9	0.0524	0.2293	0.0444	0.1869	0.0333	0.2026
282.2	0.0485	0.2238	0.0418	0.1809	0.0311	0.1948
365.2	0.0467	0.2214	0.0408	0.1783	0.0302	0.1913
456.2	0.0451	0.2332	0.0398	0.1882	0.0293	0.2019
546.9	0.0442	0.2269	0.0394	0.1839	0.0289	0.1975
686.6	0.0414	0.2133	0.0371	0.1739	0.0272	0.1874
898.8	0.0464	0.2045	0.0422	0.1687	0.0309	0.1931
1062.8	0.0480	0.2321	0.0439	0.1956	0.0322	0.2154
1206.9	0.0465	0.2316	0.0426	0.1972	0.0313	0.2190
1422.8	0.0443	0.2156	0.0407	0.1852	0.0300	0.2071
1592.7	0.0436	0.2083	0.0402	0.1803	0.0297	0.2029
1824.4	0.0440	0.2031	0.0407	0.1778	0.0302	0.2020
2028.0	0.0441	0.1991	0.0409	0.1760	0.0305	0.2061